MONASH MOTORSPORT

FINAL YEAR THESIS COLLECTION

Development of the Aerodynamic Design Tools & Processes for Formula - SAE

Ryan Ockerby - 2015

The Final Year Thesis is a technical engineering assignment undertaken by students of Monash University. Monash Motorsport team members often choose to conduct this assignment in conjunction with the team.

The theses shared in the Monash Motorsport Final Year Thesis Collection are just some examples of those completed.

These theses have been the cornerstone for much of the team's success. We would like to thank those students that were not only part of the team while at university but also contributed to the team through their Final Year Thesis.

The purpose of the team releasing the Monash Motorsport Final Year Thesis Collection is to share knowledge and foster progress in the Formula Student and Formula-SAE community.

We ask that you please do not contact the authors or supervisors directly, instead for any related questions please email info@monashmotorsport.com

DEVELOPMENT OF THE AERODYNAMIC DESIGN TOOLS & PROCESSES FOR FORMULA-SAE

RYAN OCKERBY

23366907

SUPERVISED BY: DR. SCOTT WORDLEY

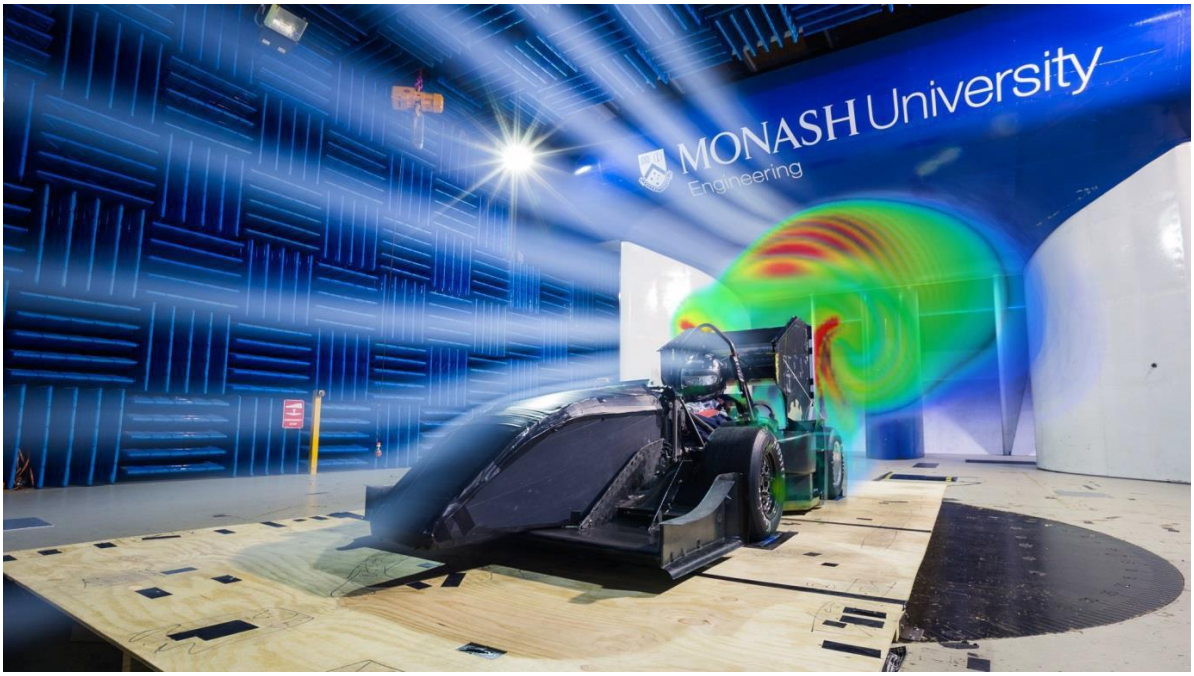

SUMMARY

This project is aimed at improving Monash Motorsport's aerodynamic package design process due to new rules and increasing time restrictions. To achieve this, faster solving computational fluid dynamics (CFD) simulations running in conjunction with highly complex cornering CFD simulations, quality wind tunnel modelling and data acquisition plus improved on-track testing were investigated.

The project was successful in that a 59% reduction in solve time for the symmetrical straight line CFD simulation from changing the domain size, model simplification and re-evaluating the convergence criteria. Post processing results has been streamlined with quicker state files and a more intuitive and fluent process of documenting on the Monash Motorsport's Google Wiki has been implemented. The introduction of a stiffer rig and larger and higher quality ground plane which showed had flow coming through the undertray is a positive step towards correlation. Tripping the flow on the stationary wheel in the wind tunnel had excellent correlation with CFD and literature.

These successes helped Monash Motorsport design their aerodynamics package with greater confidence in results and allowed for a greater number of designs and investigations to be completed.

TABLE OF CONTENTS

Development of the aerodynamic design tools & processes for formula-SAE 1
Ryan Ockerby 23366907 1
Supervised By: Dr. Scott Wordley 1
Summary 1
Table of Contents 3
1. Introduction 6
1.1 Background to Formula-SAE Aerodynamics 6
1.2 Project Motivation & Aim 7
2. Design Process 9
2.1 Methodology 9
2.2 CFD Post Processing & Reporting 11
2.2.1 Google WIKI Documentation 11
2.2.2 .CST Files for Individual Parts and Full Car 14
2.3 Data and Server Management 15
3. Symmetrical CFD Model 17
3.1 Initial Analysis of previous CFD model 17
3.1.1 Detailed Analysis of Component Forces 17
3.1.2 Turbulence Modelling 19
3.1.3 Y+ Plus Values 20
3.2 Ahmed Body 22
3.3 Domain Studies 23
3.3.1 Nearfield 25
3.3.2 Wake 28
3.3.3 Farfield 31
3.3.4 Future Domain Setup 31
3.4 Mesh 32
3.4.1 Mesh Setup 32
3.4.2 Future Work 33
3.5 Boundary Conditions and Expressions 34
3.6 Model Simplification 35
4. Asymmetric Model 37
5. Rotating Reference Frame (RRF) 40
5.1 Motivation 40

5.2 Additions to the Navier Stokes Equations 41
5.3 Model Setup 41
5.4 Future Work 43
6. Wind Tunnel Testing 44
6.1 Ground Boundary Layer 44
6.2 Tunnel Testing Rig and Groundplane 44
6.3 Wheel Tripper 46
6.4 Blockage Effects 46
6.5 Driver Model & Height 46
6.6 Testing Rear Endplates 47
6.7 Flow Visualisation 47
6.7.1 Wool Tuffs 47
6.7.2 Smoke 48
6.7.3 Surface Streamlines 48
6.8 Future Work 49
7. On-Track Testing 50
7.1 Pressure Tapping 50
7.2 Physical & Quantitative Data 51
7.3 Future Work and Concepts 51
8. Conclusions 52
9. Acknowledgements 52
10. References 53
11. Appendices 54
11.1 Complete Table of Force Standard Deviation 54
11.2 Graphs showing force residuals and standard deviation 55
11.3 New CFD Run Template 59
11.4 Size of Aerodynamics CFD Run Folder 61
11.5 Ahmed Body 61
11.6 Domain Studies 62
11.7 Rotating Reference Frame Setup Spreadsheet 63
11.8 Wind Tunnel Testing Report 63
11.9 Wind Tunnel Schematic 68

Nomenclature

μ_t	Turbulent viscosity value (Pa/s)
μ	molecular dynamic viscosity (Pa/s)
μ_t / μ	Eddy Ratio
CL.A	Coefficient of Lift. Area
ρ	Density (kg/m^3
v	velocity (m/s)
L	Lift (N)
D	Drag (N)
C_P	Coefficient of Pressure
p	Pressure (Pa)
p_∞	Freestream pressure
v_∞	Freestream velocity
M_Y	Moment about Y axis (Nm)
M_X	Moment about X axis (Nm)
M_Z	Moment about Z axis (Nm)
$F_{Coriolis}$	Coriolis Force (N)
$F_{Centrifugal}$	Centrifugal Force (N)
$\vec{\omega}$	Angular Velocity (rad/s)
Ro	Rossby Number
U	Freestream RRF velocity (m/s)
l	Distance (m)
Re_x	Reynolds number
δ	Boundary Layer Thickness (m)

1. INTRODUCTION

1.1 Background to Formula-SAE Aerodynamics

Formula-SAE (F-SAE) is the largest international engineering design competition and is held in over 10 countries with over 500 teams participating. Students design, manufacture and test prototype open wheeled cars against other universities across seven events that test the vehicles performance, design, cost and business model in which points are totaled to out of a possible 1000 to determine the overall winner. The Society of Automotive Engineers (SAE) set rules in which teams must design their car around to ensure safe vehicle design and close competition.

Monash Motorsport, Monash University's entrant, has been competitive in aerodynamic design in Formula Student since 2002. Aerodynamic performance through the use of aerodynamic components such as wings, underbody diffusers and bodywork has been a long-debated topic because of the low-speed tracks Formula Student competes on. Majority of the teams chose to run without additional aerodynamic components before 2013. Taking advantage of this through access to the Monash Wind Tunnel and knowledge aerodynamic engineering, Monash won the past six Formula SAE-Australasian competitions and placed highly in competitions in the United Kingdom and Germany.

Figure 1.1: The Evolution of Formula SAE - Formula Student Germany 2006 on the left with 3 teams using aerodynamic components and 2014 on the right with ~80% of the teams using aerodynamic components.

Since 2013, aerodynamic components are seen on the majority of teams competing (Figure 1.1). The increasing amount lead SAE to change the rules regarding aerodynamic packaging space and mounting to prevent incidents with large wings failing and falling off the car whilst also challenging students to design from first principles. These rules meant that wing span on the rear was reduced by over 40% and restricted height forward of the front wheels. In order for Monash to retain their aerodynamic advantage over their competitors, current and future designers of the aerodynamic components must ensure the design processes they use directly translate to performance on-track.

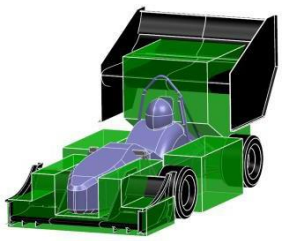

Figure 2: The 2015 rule packaging space (within the highlighted green areas) and Monash's 2014 aerodynamic design.

1.2 Project Motivation & Aim

In order to score a significant increase in points over other competitors, a point simulator was created for the Monash F-SAE team (Webb, 2012). It was determined that a 10% increase in downforce would result in a 15 point increase out 1000 available at the competition (Mapson, 2011) and is represented in Equation 1:

$$Points * CL.A = \frac{0.86 \cdot |L|}{\rho v^2} \ldots (Eq.1)$$

Computational Fluid Dynamics (CFD) has been the main design tool used to develop aerodynamic components since 2011. This was driven by reduced wind tunnel testing time, shorter design periods and earlier build completion dates to enable the car to be set-up and ensure reliability for competition. The consequences of such design processes are that there is no ability to modify the design if wind tunnel and on-track testing show discrepancies against the CFD simulation results as the components have already been manufactured.

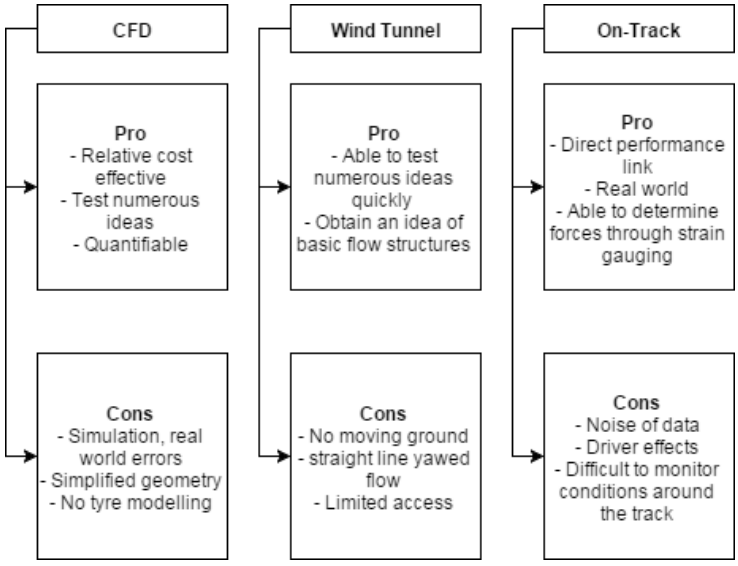

Flow Chart 1: Benefits and drawbacks of each major design tool.

The new design process aims to incorporate all three major design tools into the design and allow for modification to manufactured components and data for future years and design event. A CFD simulation model that enables the designer to quickly change concepts and parameters in conjunction with a complex and high quality CFD simulation model ensure flow structures are consistent and accurate. Improving the wind tunnel model so it can correlate with CFD results will also help integrate the three tools.

To achieve the desired design process, three aspects needed to be addressed:

- Reduction in solve time through domain dependence studies and model simplification to allow for more simulations to be completed during the design period
- Ensuring quality correlation between wind tunnel and on-track testing with CFD
- Implementing cornering simulations using asymmetric models and rotating reference frames to design the car for yawed flow

1.3 Literature Review

Race Car Aerodynamics (Joseph Katz) / Competition Car Aerodynamics (Simon McBeath)

These books provided a broad and detailed approach to designing external aerodynamics of racecars. They are slightly outdated and therefore the computational side isn't applicable but on-track and wind tunnel testing provides insight into ground planes and pressure tapping.

Monash Motorsport Final Year Projects

These papers provide an excellent background into point simulation (Webb, Mapson, Bett), previous aerodynamic studies (Wordley, Phersson, McArthur, Buckingham) and how these effect on-track performance (Juric, Russouw, Salvo).

LEAP Australia Blogs

LEAP Australia, industry leaders in computational simulation, provide detailed and informative blogs on many aspects of computational fluid dynamics with ANSYS.

FSAE Rules

The rules set out by the SAE committee have affected the aerodynamic packaging size, hence learning the motivations and reasoning behind these rule changes was motivation for the project.

Ahmed Body Papers

Numerous papers exist and have been reviewed on this as it was the old industry standard. Numerous CFD simulations have correlated their results with those found on the Ahmed Body during wind tunnel testing.

2. DESIGN PROCESS

2.1 Methodology

Previous Monash aerodynamic packages have been designed exclusively through CFD, with wind tunnel testing and on-track testing being used as methods of validation to CFD. This method is shown in Figure 3. The issue with this design methodology presents is no modifications can be made to the aerodynamic package if there is a difference between the two testing conditions and CFD. All testing methods have shortcomings, as mentioned throughout this report. By allowing future aerodynamic design engineers use all three tools effectively and together, an improved correlation between the design tools will progress the team towards the highest performing design.

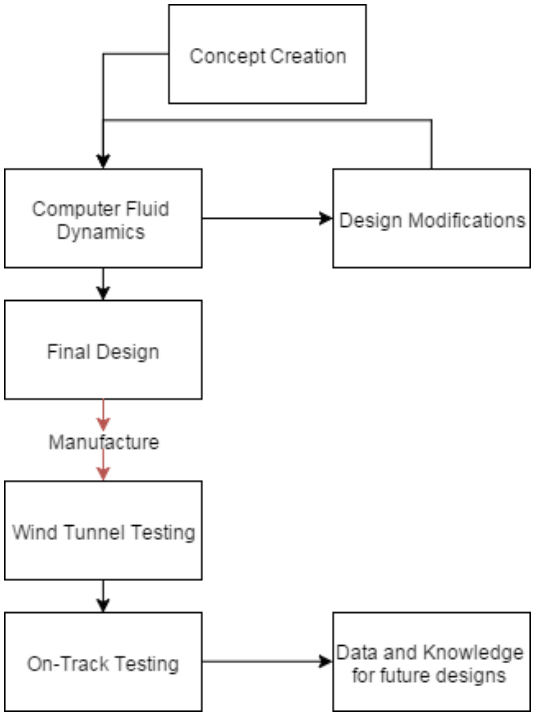

Figure 3: 2013 Design Process.

The 2013 design process was an example of this previous design methodology. Over 180 symmetrical straight-line CFD simulations were completed during the three month design period. It can be seen from Figure 4 that initially there were large fluctuations on the performance of the package. The reason for this is that other parameters outside an aerodynamic part designer's control, such as chassis and suspension geometry and other concept based design decisions, are constantly changed through the first month of the design period. This period is used by the aerodynamic team to quickly evaluate new concepts and innovations, hence the large deviation of the results.

Once this initial period is completed and a concept is decided on by the other sections, the performance of the design steadily increases. This was due to the designers increasing their knowledge about how to manage the flow across the car and sweeping through certain parameters and progressing with the highest performing run.

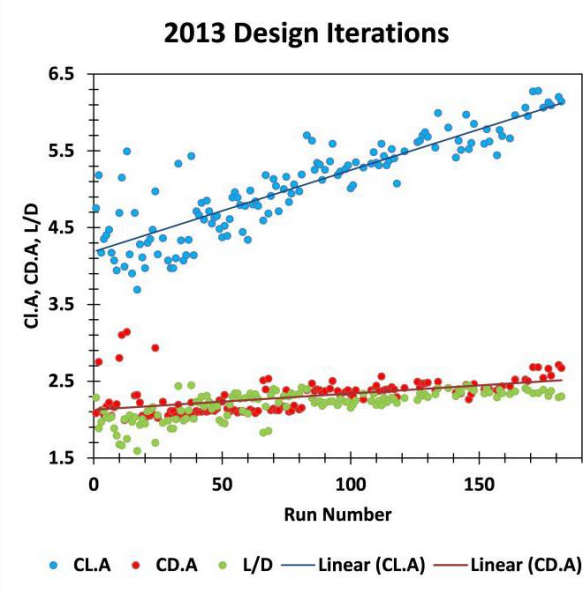

Figure 4: The 2013 Design Process. Note the linear relationship between number of iterations and CL.A.

This issue of completing all simulations in a symmetrical straight-line model is that cornering and yawed flow is not taken into account in the design. Previous studies have shown a large difference in flow structures (see Section 5 – Rotating Reference Frames) and therefore components that affect the yawed flow (endplates and strakes) reduce the effectiveness of the package in this mode.

The process of making major components out of MDF and plywood, for example endplates, for wind tunnel testing has resulted in those parts not being able to drive on-track at the same time. Due to timelining of the overall car, the endplates need to be constructed before wind tunnel testing starts. This timelining and manufacturing process forces the team to make the final endplates before wind tunnel testing begins and therefore modifications to the final design cannot be made.

To resolve the issues of designing for pure straight line and not being able to modify and correlate the aerodynamic package after the final design is determined, a new process was implemented for 2015 and future years. The process is summarized in Figure 5:

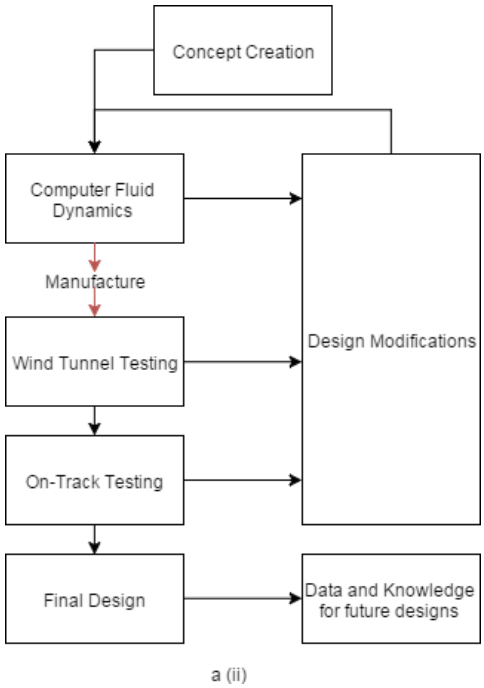

Figure 5: Proposed Design Process.

This process incorporates all three major design tools before the final design is determined. Within this new methodology, there are also minor aspects that have been changed:

- During the concept stage, a quick symmetrical CFD model will be used to evaluate a high number of aerodynamic innovations and car concepts. With more iterations being used, the aerodynamic designers will gain a greater understanding of where to baseline from after the overall car concept is determined.
- After a concept is determined, cornering simulations (both asymmetric and rotating reference frame) will be conducted when a new baseline is created.
- The wind tunnel CFD model will be used prior to wind tunnel testing to evaluate concepts that may require large amount of manufacturing time.
- Designs that performed well in the wind tunnel and weren't in the initial CFD baseline must be compared in both symmetric CFD model and wind tunnel model
- Components such as endplates and diveplates are to be made out of fiberglass to enable the designers to modify them in both the wind tunnel and on-track. This reduces the impact on human resources and time consumption from previous methods. The final design can then be determined.
- The method of splitting up the runs to each part designer and then combining the best results will be kept as this has proven to be an excellent method of progressing the design.

3. SYMMETRICAL CFD MODEL

The symmetrical CFD model uses half the car, split from the Y-axis, to simulate the forces and flow structures on the car when travelling in a straight line.

Currently there isn't any standard design for the domain and meshing for any vehicle, as it depends on the users preferences on computational power, time and accuracy requirements. The geometry, speed and Reynold's number are also factors in this design. Therefore techniques and theories produced from previous studies of designing domains and meshes for cars will be incorporated into this project as well as new techniques developed through design and testing.

3.1 Initial Analysis of previous CFD model

3.1.1 Detailed Analysis of Component Forces

To understand the current flow structures and their corresponding forces across the car, as well as the effect of the domain and meshing techniques a comprehensive study was conducted on the 2015 CFD model created by the Monash 2015 Aerodynamics team. The standard forces that are output total to seven different components: front wing, rear wing, undertray, front and rear wheels, body and radiator. Having only these components that group smaller components together makes it difficult to determine where instabilities are and where to best place higher resolution mesh effectively.

In order to improve this analysis and identify the components causing certain flow structures, a total of 62 components and sections of major components was selected as seen in Figure 12. These were analyzed and run through a CFD simulation.

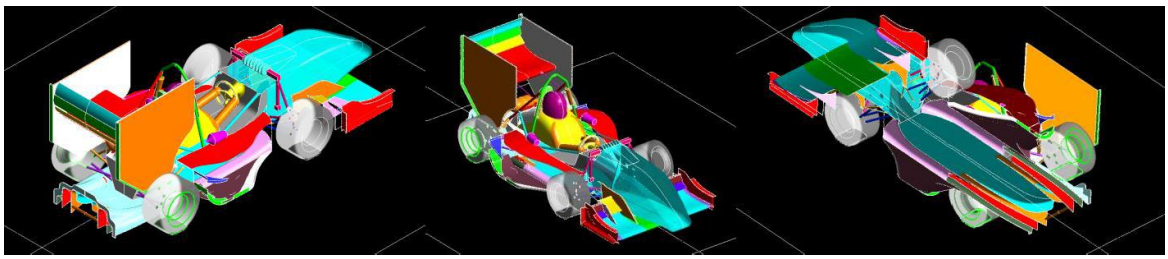

Figure 12: Three angles showing the different components (varying colours) that were analyzed for forces and residuals across the 2015 Monash F-SAE Car.

An example of why these sections need to split up is shown below. The driver's head experiences a large velocity gradient though it had no inflation layer or mesh refinement. The helmet and body must then be evaluated to determine whether increasing the mesh resolution is going to increase the quality of the simulation against increasing solve time.

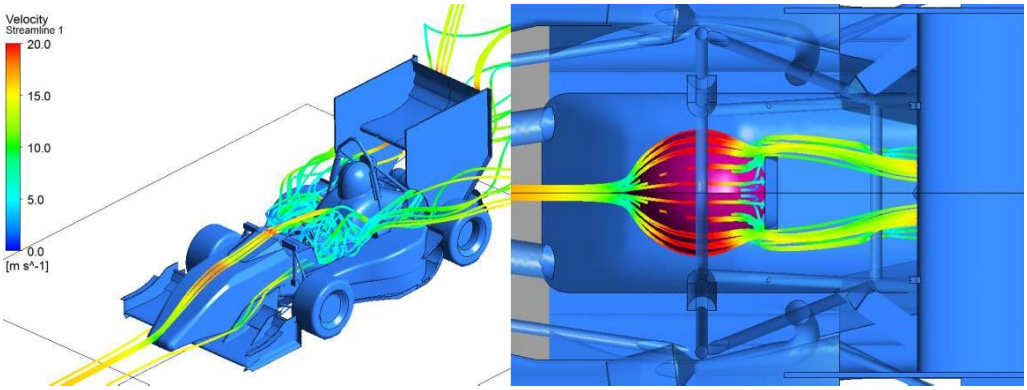

Figure 13: The left showing velocity streamlines (forward and backward) from the cockpit. The right shows streamlines (forward and backward) from the helmet. Both of these components experience high velocity gradients and separation of flow but don't have localized mesh refinement

Conducting this simulation has allowed us to identify sections of the car that will need localised mesh refinement studies completed on them. Using graphs such as those shown in Figure 14, it was seen that the simulation coverges to a general range after 300 iterations. This has been consistent with the multiple studies completed on different geometry. Stopping the simulation at a consistent 300 iterations instead of the current 400+ iterations since the simulation doesn't converge to 1.0e-4 range as inputted into the convergence conditions will save approximately 6 hours from the current 24 hours. Consideration into stopping at a specific iteration will be taken by checking the force residuals of after each run.

It is recommended to future designers that when completing a run that the force residuals are saved into the 'Results' folder so if there is any unsteadiness, it can be recorded and used to evaluate the performance of the design. The FIGURE and TABLE below show this resolution.

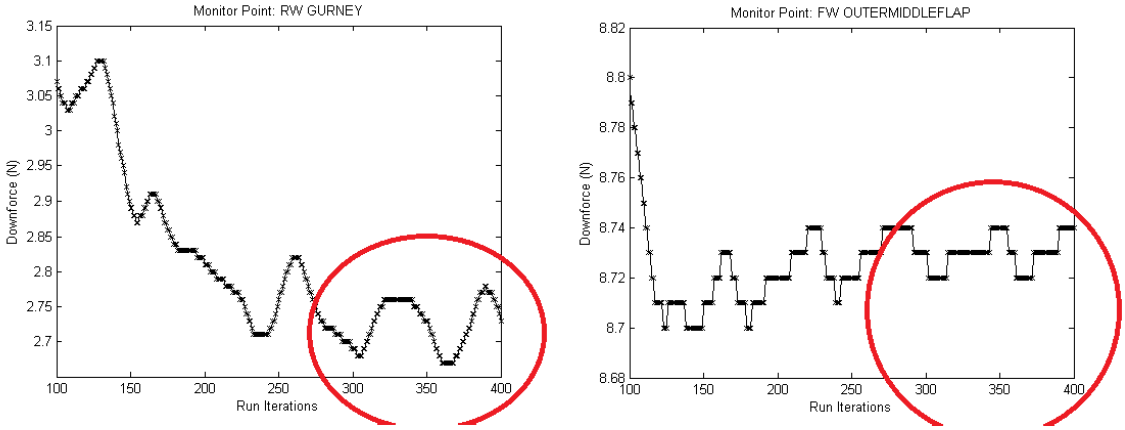

Figure 14: (a) Downforce of Rear Wing Gurneys after CFD run iterations. (b) Shows the same graph but with the Front Wing Outer Middle Flap. Both show general convergence after approximately 300 iterations. Appendix B shows all of the downforce versus run iteration

Table 1 shows the components that had the largest standard deviations of the 62 components that were analyzed. Standard deviations of the downforce values over 50 iterations from 100 to 400 iterations were tabulated and 250 to 400 are also shown. As expected, the undertray and front wing were a major influence in the instabilities of the residual force due to these components being in

high unstable pressure gradients with transverse flow and vortices interacting with each other. These pressure gradients and vortices are difficult to capture without becoming unstable.

Table 1: The standard deviation (STD) and percentage change of the STD of iterations 250-300, 300-350 and 350-400. The red (highest value) to green (lowest value) scale shows the magnitude of the vlaues for each column.

Parts	STD 250-300	Δ% 200/300	STD 300-350	Δ% 250/350	STD 350-400	STD Total Score
Front Wing (FW)	1.13	36.10	0.83	20.32	1.04	1.09
FW Mainplane	0.31	10.92	0.28	7.18	0.31	0.33
FW Mainplane Flap Section	0.40	7.32	0.37	10.05	0.42	0.48
Rear Wing (RW)	0.76	1.85	0.77	13.55	0.89	1.53
RW Flap 1	0.12	19.92	0.16	9.55	0.17	0.31
RW Mainplane	0.50	0.15	0.50	41.26	0.86	1.09
Nosecone	0.14	16.80	0.17	45.04	0.12	0.21
Intercooler Flow	0.33	42.26	0.58	24.49	0.76	1.54
Radiator Flow	0.62	9.79	0.57	21.34	0.72	1.99
Sidepod Edge	0.03	47.02	0.02	20.21	0.02	0.22
Sidepod Top Surface	0.21	14.41	0.18	20.53	0.23	0.23
Sidepod 2	0.25	12.04	0.22	19.73	0.27	0.32
Undertray (UT)	0.72	35.70	1.12	16.81	0.96	1.00
UT Inboard Tunnel	0.10	26.19	0.13	15.86	0.11	0.22
UT Outboard Section	0.08	36.32	0.13	22.68	0.10	0.29
Front Downforce	2.12	15.64	1.83	1.44	1.86	2.65
RearDownforce	2.03	21.02	2.57	4.10	2.68	3.76
TotalDrag	0.85	23.59	1.11	26.04	0.88	1.70
TotalDownforce	0.79	31.03	1.15	3.27	1.11	2.02
Total	11.51		12.70		13.53	20.98

The rear downforce also oscillated considerably more than the front downforce. Being downstream from the front of the car, these instabilities will carry on as they progress further downstream.

The decision to stop at 300 iterations can also be reiterated through the total variation of the forces. The averaged value of the total forces from 100 iterations to 400 is within 0.06% of the final value at 400 iterations.

3.1.2 Turbulence Modelling

The Reynolds Averaged Navier Stokes (RANS) approach is currently used by the Monash Motorsport team. The decision to run RANS is made simply because other advanced simulations, such as Large Eddy Simulations (LES) and Scale Adaptive Simulation (SAS), are too complex and resource expensive to undertake.

The RANS model deconstructs the Navier Stokes and conservation equations, Figure 15, where the velocity is split into its average and fluctuating components (LEAP Australia, 2012). The remaining value is the Reynold's Stress which is resolved using an isotropic value for the turbulent viscosity value,μ_t and is termed the Eddy Viscosity Model.

The Shear Stress Transport model is the industrial standard and used by Monash Motorsport. It combines the use of the two equation models, k-ε and k-ω, which is then applied for different sections of the model. The k-ε model is used in the free stream section of the model as it is has excellent properties with non-wall bounded flow. The k-ω equations is used near the surface of the car and ground as it predicts wall bounded flows better than k-ε.

Continuity $\frac{\partial \rho}{\partial t} + \frac{\partial}{\partial x_i}(\rho u_i) = 0$

Momentum $\frac{\partial}{\partial t}(\rho u_i) + \frac{\partial}{\partial x_j}(\rho u_i u_j) = -\frac{\partial P}{\partial x_i} + \frac{\partial \tau_{ij}}{\partial x_j}$

Energy $\frac{\partial}{\partial t}(\rho h_{tot}) + \frac{\partial}{\partial x_j}(\rho h_{tot} u_j) = \frac{\partial P}{\partial t} + \frac{\partial}{\partial x_j}(u_i \tau_{ij} + \lambda \frac{\partial T}{\partial x_j})$

where $\tau_{ij} = \mu\left(\frac{\partial u_i}{\partial x_j} + \frac{\partial u_j}{\partial x_i} + \frac{2}{3}\delta_{ij}\frac{\partial u_i}{\partial x_j}\right)$ $\quad h_{tot} = h + \frac{1}{2}u_i^2$

Figure 15: Navier Stokes Equations and Conservation Equations (LEAP Australia, 2012).

3.1.3 Y+ Plus Values

The Y+ plus is essential in mesh generation and its accuracy. This is a non-dimensional value that determines the distance between the first mesh node from the surface of the part or wall. This value needs to be of less magnitude than the boundary layer thickness otherwise incorrect values in pressure gradients and velocity will arise. This relates to the inflation layer in mesh creation in such that there is enough inflation layers within this boundary layer thickness.

Due to the high level of pressure gradients which leads to a high possibility of flow separation, the designer must ensure that the boundary layer is captured near the surface with a quality resolution mesh. It is recommended that baseline runs need to include Y+ contours in the generated reports to ensure that the model is accurate. From Figure 16 (Cebed, 2013) below, values of Y+ that are less than 10 represents the flow in the viscous sublayer with lower inertial forces. This is the low-Re region and is important for pressure gradients and separation.

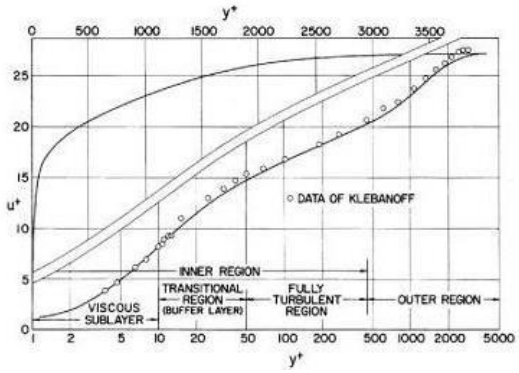

Figure 16: Mean velocity distribution across a turbulent boundary layer with zero pressure gradients (Cebed, 2013).

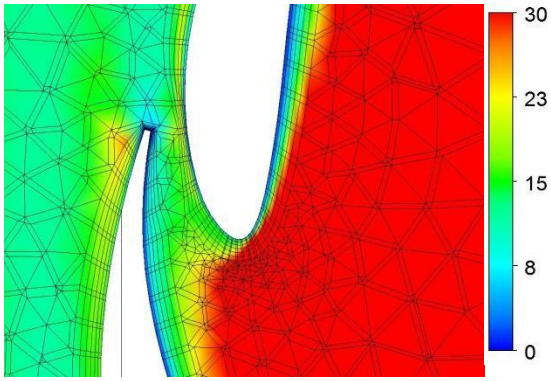

Figure 17: The Eddy Viscosity Ratio on the second and third flaps on the rear wing.

From Figure 17, it can be seen that the boundary layer transitions into the logarithmic region outside of the inflation layer. Due to capturing the laminar sub-layer in high detail, the boundary layer is not accurate which will affect pressure gradients and forces. The examples of good mesh capturing the boundary layer and laminar sub-layer and bad mesh can be seen in Figure 18. The y+ needs to be increased in this region and hence inflation layer height.

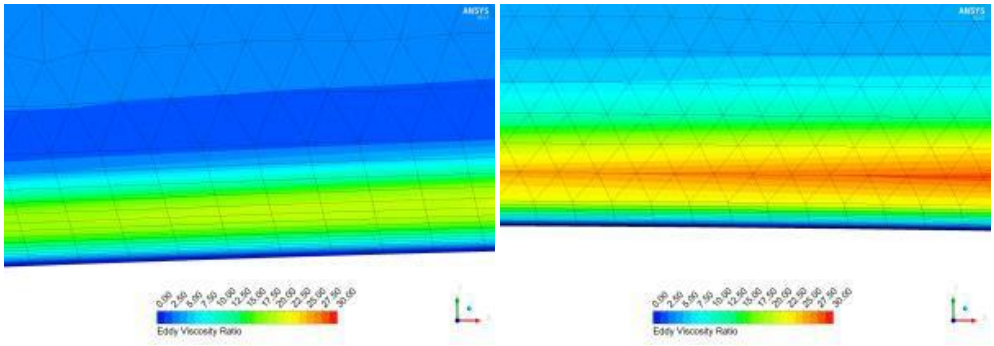

Figure 18: Eddy Viscosity Ratio on a demonstrative surface. The left demonstrates a good example of inflation layer whilst the right is a poor example (LEAP Australia, 2012).

Analysing the Y+ values across the car showed that there is a requirement to apply mesh refinement and inflation layer on the body and helmet in the CFD model. As Figure 20 shows, the helmet and body are well over 150 (maximum value is nearly 600) which is considerably outside the range that the model requires to achieve of approximately 30. It can also be seen that the wheel could also require a finer mesh as it approaches a 100 y+ value. Applying an inflation layer would improve the accuracy of these results on this section.

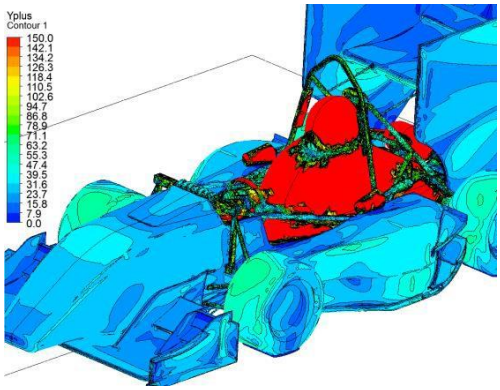

Figure 19: Y plus values across the car model. Note the high y plus values on the helmet and body.

Half of the elements in the mesh are tetrahedrons in the Nearfield and less than 15% of the total elements are prism elements. Therefore adding more prism inflation layers would contribute to more elements but the improved accuracy, especially around the helmet and body which influences the rear wing flow, could allow for improved design considerations for geometry modelling and rear wing flow.

3.2 Ahmed Body

An Ahmed body is a bluff body that is used to simplify a vehicle in close ground proximity (S.R. Ahmed). Numerous studies have been conducted on this body in both wind tunnels and CFD simulations and therefore can compare with design techniques that are successful in this application.

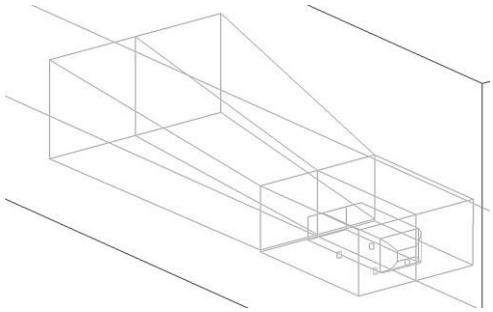

Figure 20: Ahmed Body with scaled CFD domain.

The model used for the results in Table 2 was the current CFD model for the 2015 Monash car. Results with other domain dimensions, including a small scale domain using the dimensional ratios of the current car model to the domain and a full model (Figure 20) using the same small scale dimensions, was also completed.

Comparison showed excellent correlation between the wind tunnel data from the Ahmed studies and the CFD simulations. This is represented in Figure 21, therefore basic flow structures with simple force calculations can accurately be determined from the CFD simulations. Introducing more complex geometry will further progress the model away from key and transferrable results with the Ahmed body but the concept has been proven.

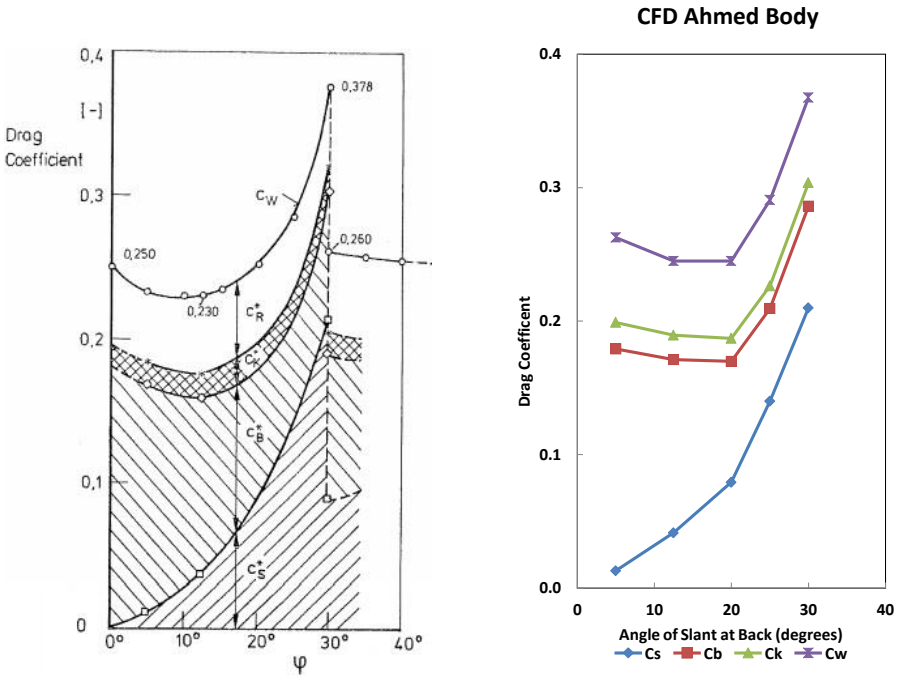

Figure 21: Original Ahmed Body results from wind tunnel testing (left) and simulations in Monash Motorsport's fluid domain (right).

The flow structures represented in Ahmed Figure 22 are seen in the CFD results. There are five main flow structures: the major horseshoe vortex forming off from the top side edge of the body, the ground bubble region, two recirculation regions on the back face and the attached flow that gets drawn into the horseshoe vortex from the slant face. All five flow structures are present in all the studies of varying slant angles with varying amount of strength for each.

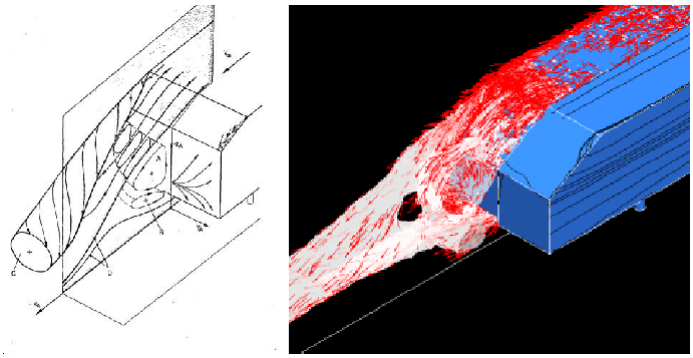

Figure 22: Ahmed Body in scaled dimensioned full domain (right) and showing similar horseshoe flow structures to that of Fig 6 in Ahmed, 1984 (left).

3.3 Domain Studies

The fluid domain is grouped into three regions shown below in Figure 23: Nearfield, Wake and Farfield. Each region was modified to determine the best effective size with solve time and convergence the main considerations. The baseline fluid domain Nearfield accounts for 77.2% of the elements within the simulation, the Farfield 13.6% and the wake box 9.2%.

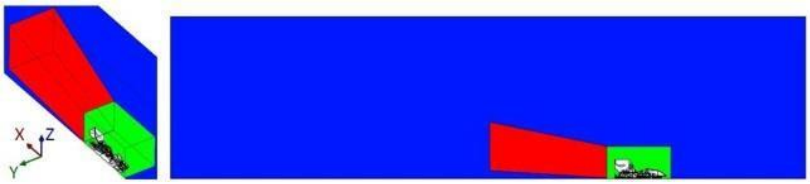

Figure 23: Fluid Domain Setup: White = Car, Green = Nearfield, Red = Wake and Blue = Farfield.

Studies showed that there was almost a linear relationship with solve time and number of elements, shown in Figure 24. Any method of reducing the number of elements will be beneficial to the designers as this can increase the number of simulations that can be completed during the design period.

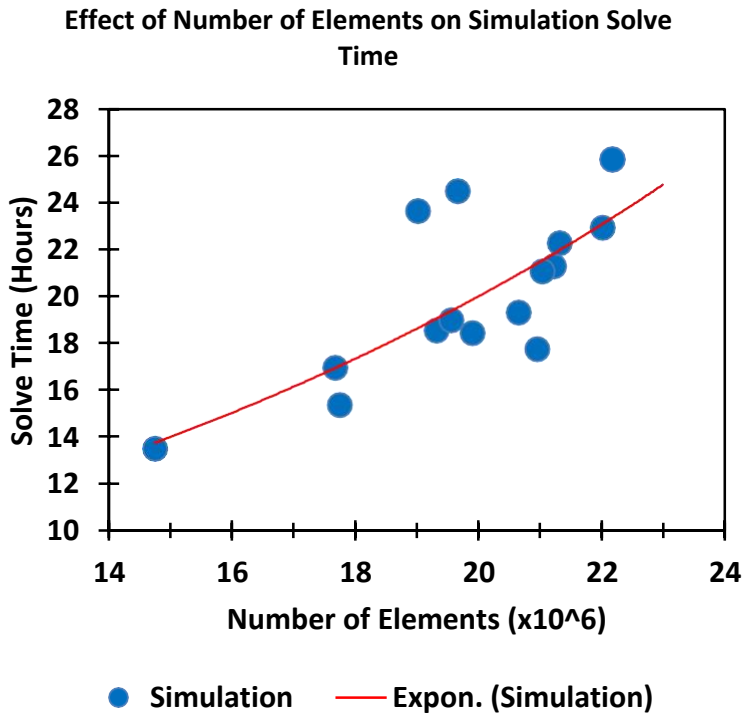

Figure 24: Reducing the number of elements has an almost linear relationship with solve time.

When conducting these sweeps, it was ensured that the results weren't being affected by the changing domain. In order to do this, runs were compared to different model baselines and the domain sweeps were swept in greater than and less than the original domain size for convergence reasons. Figure 25 shows the body and rear wing were the components that showed the largest percentage difference to the baseline runs. This was theorized to be due to small changes in upstream flow can greatly affect the rear sections of the car and also the large effect the rear wing has on the Wake region and the Nearfield region in both height dimensions.

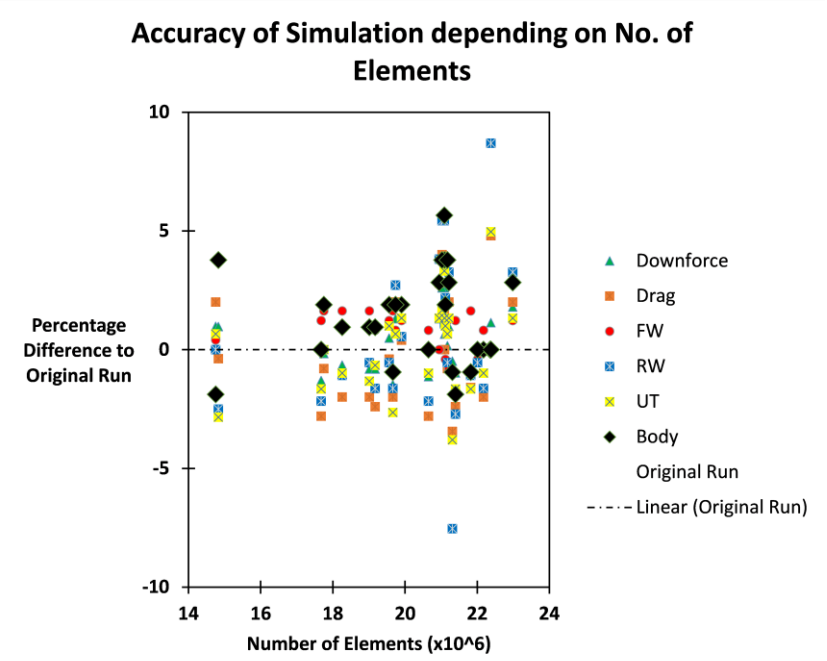

Figure 25: Percentage difference the simulations were to their solver baselines with relation to number of elements.

3.3.1 Nearfield

The Nearfield provides a maximum 30mm tetrahedral meshing in order to capture the high pressure gradients and flow structures close to the vehicle. Due to the relatively small mesh size in this region, it accounts for 77.2% of the total elements and therefore a large amount of meshing and solve time can be reduced if the spatial size of the Nearfield is reduced.

Numerous studies were conducted on the Nearfield, varying both shape and size. A rectangular prism was found to be the most efficient shape as it allows for simple control of size variation and mesh arrangement compared to a cylinder and other shapes.

Changing the width of the Nearfield was the most effective method of reducing the spatial size without affecting the flow field. Due to large deviations in the flow being in the X and Z directions, the flow in the Y direction isn't disrupted and therefore a narrower Nearfield can be used whilst keeping the same flow structures and forces as the baseline run. The new Nearfield width has a solve time that is 30% less than the baseline.

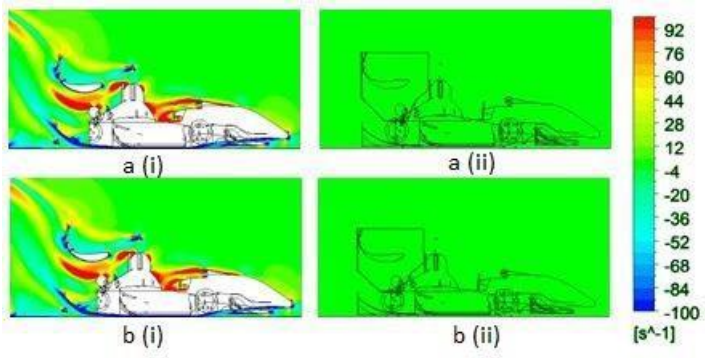

Figure 26: Shows the vertical gradient of the streamwise velocity (∂u/∂z) at planes in ZX at Y=0 for simulations a (i) (Baseline) and b (i) (narrow Nearfield) and at Y=1m for a (ii) (Baseline) and b (ii) (narrow Nearfield). There is little to no variation in the vertical gradient between the runs.

The height of the Nearfield was also varied through different baselines, with the average percentage difference to the original baselines and the size of the modification shown in Figure 27 below.

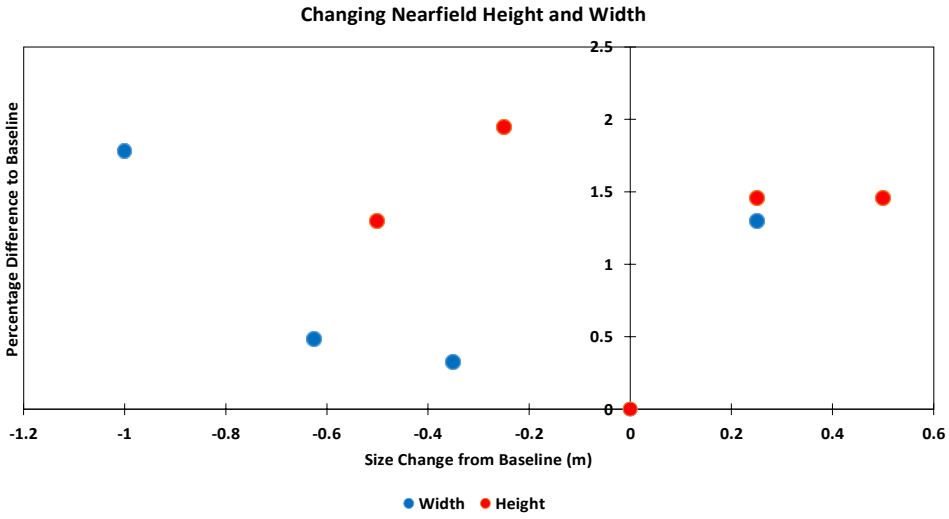

Figure 27: Accuracy of height and width of the Nearfield.

As discussed above, the height was more sensitive to changes than the width. The large curvature of the flow in the Z direction results in high pressure gradients in the flow in the z direction across the span of the car. The difference of reducing the height is shown in Figure 28.

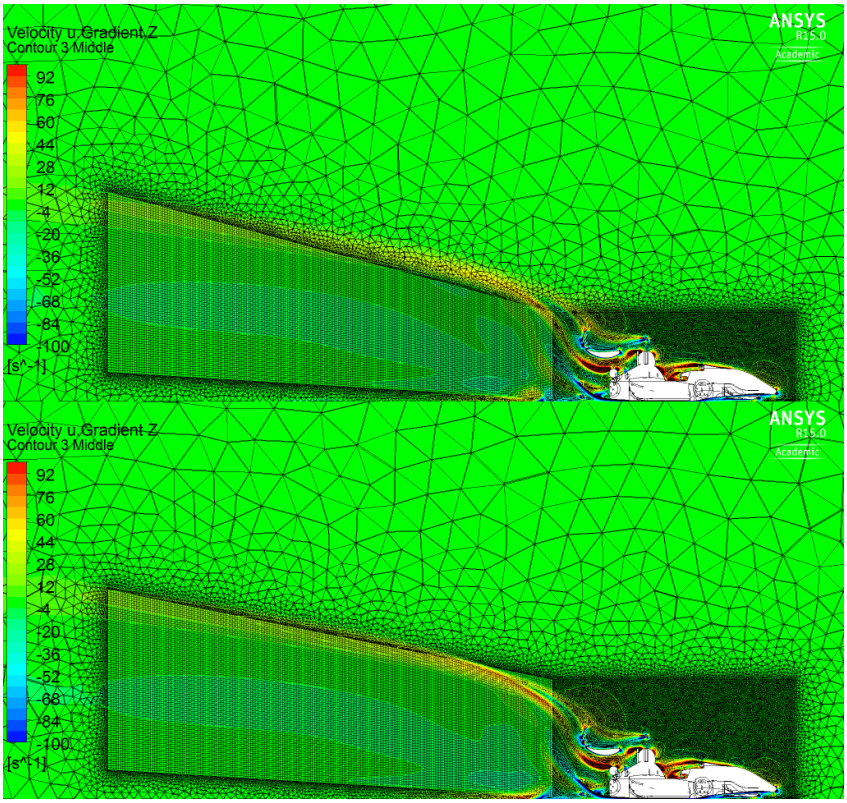

Figure 28: Difference on Nearfield Height, streamwise velocity (∂u/∂z) at planes in ZX at Y=0.

Two designs that attempted to use the height of the Nearfield at the rear wing and hence keep the same Wake region whilst reducing the frontal area of the first section of the car was the Slant Angle run and the Tight Field run.

The slant angle run had a considerable difference in front wing forces, over 30 N less than the baseline run. Figure 29 below shows as this difference through the vertical gradient in the streamwise velocity. It appears that the flow has been restricted by the reduced size of the front section of the Nearfield.

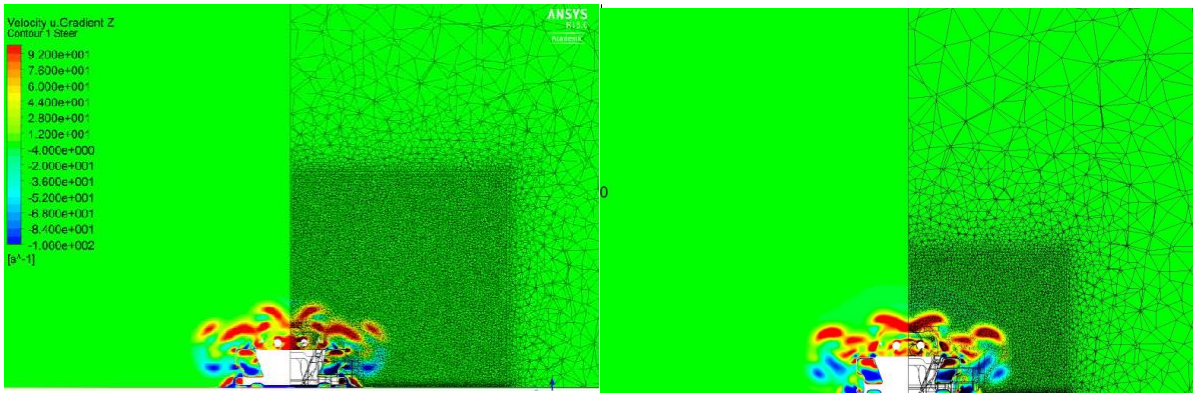

Figure 29: Baseline on left, Slant angle (top front cut back due to there not being a high pressure gradient or flow curvature, on the right. streamwise velocity (∂u/∂z) at planes in ZY at X=0.

The Tight Field run was created using a swept geometry around the high velocity gradients. This was an attempt at creating the minimum volume for the Nearfield. Unfortunately the mesh did not patch

conform to the Wake field and hence created tetrahedron elements through the wake box, increasing the total element count by 10 million.

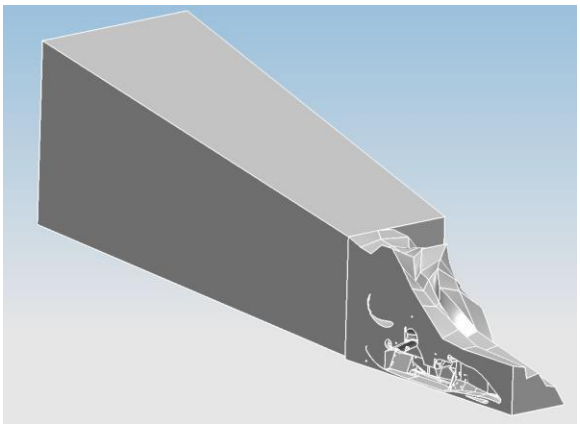

Figure 30: Failed attempt at minimum volume.

3.3.2 Wake

Changing the Wake region parameters (length, width and height) did not have a significant effect on the forces on the car. However, there was a difference in the wake itself and the magnitude of velocity gradients in the wake region.

The effect of length of the Wake region has a large effect on the length of the wake from the car. As can be seen from Figure 31, the wake is diffused by the tetrahedral elements. The same could be said about the hex elements in the Wake region in that the wake is being extended further than expected. Further studies on-track is required for this. This could be driving through a smoke field laid out on a track or fine dust and then driven through. This would give a better estimate into what length the wake box should be. The baseline length was kept for all future simulations because of this unknown factor.

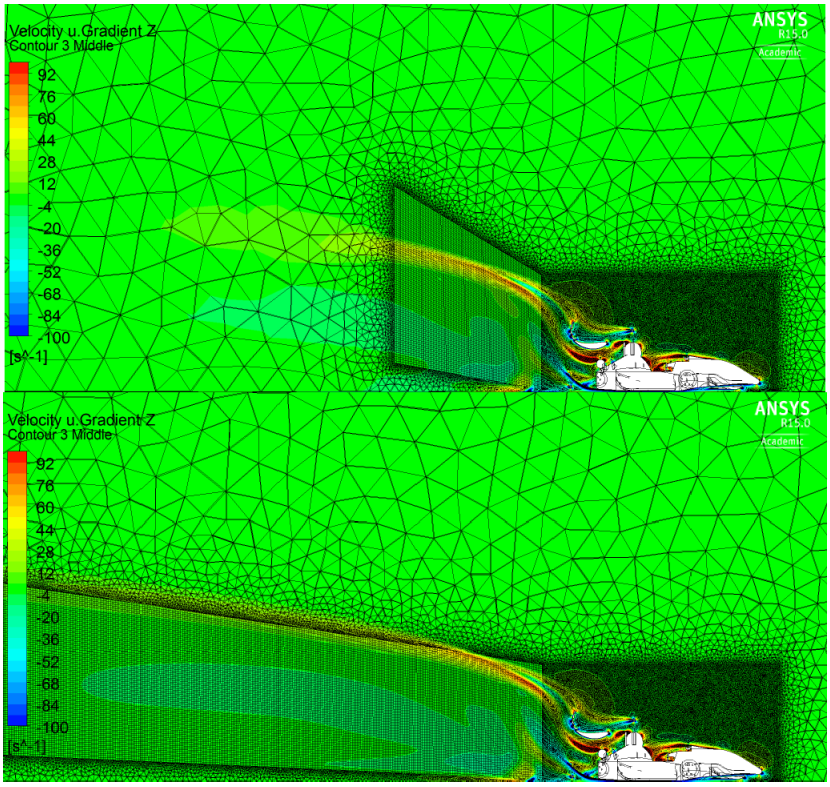

Figure 31: Changing wake region length, streamwise velocity (∂u/∂z) at planes in ZX at Y=0.

Modifying the width of the Wake region at the end of the structure had an insignificant effect on the wake flow structure. Figure 32 shows there are a slight difference from the undertray wake but are at a low-near free stream value that it can be considered negligible. As with the length dimension changes, it is not difficult to determine the correct wake region size in this direction change without knowing what the on-track wake dimensions and structures look like.

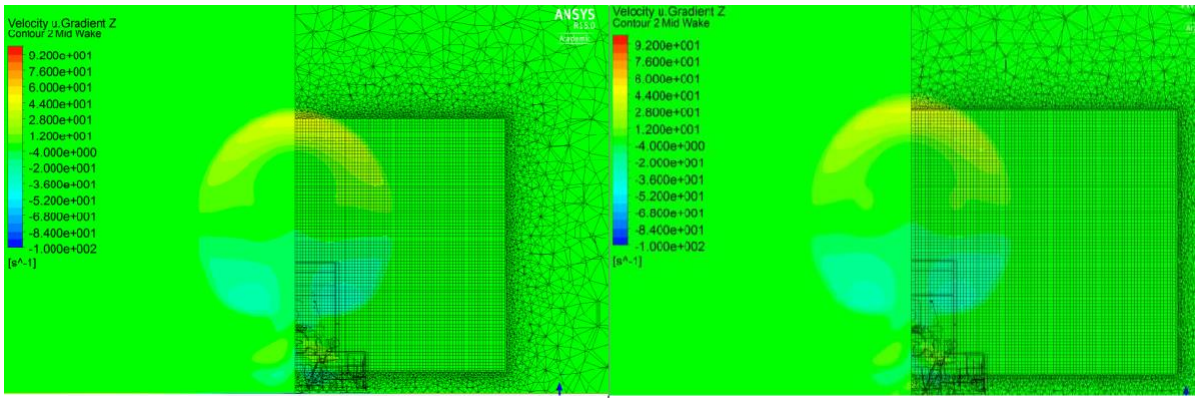

Figure 32: Comparing wake region width, streamwise velocity (∂u/∂z) at planes in ZY at X=2.

Changing the height of the Wake region had the largest effect on the flow structures in the wake. In the Figure 33 below, the increased height run captures the entire wake with higher velocity gradients whilst the decreased height shows lower velocity gradients once it reaches outside of this region. It would be better to run with this higher wake box as then the wake is in one mesh element type region rather than exceeding the limits into the Farfield region.

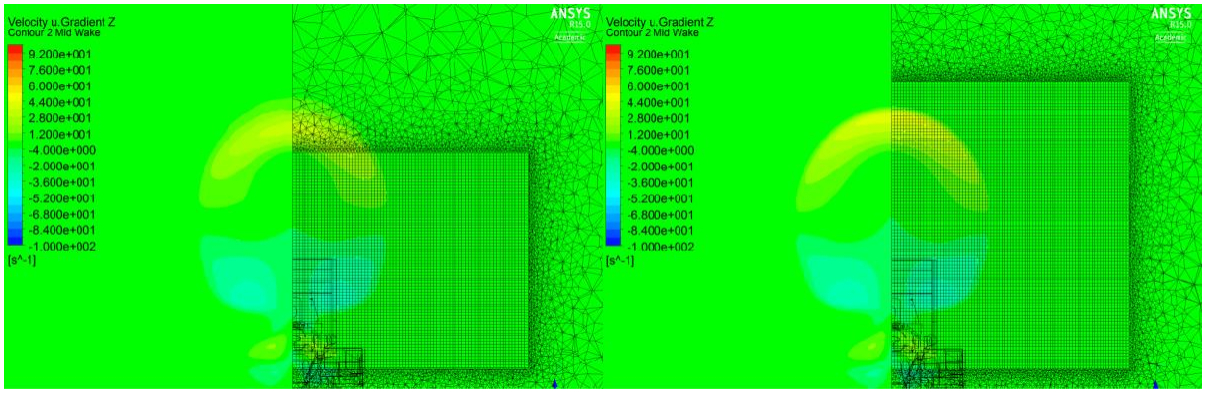

Figure 33: Changing wake region height, streamwise velocity (∂u/∂z) at planes in ZY at X=2.

To further investigate the effect of the tetrahedral elements artificially diffusing the wake, three simulations were conducted without a wake region with different car models and compared against the baselines. Again this showed the wake being reduced in length.

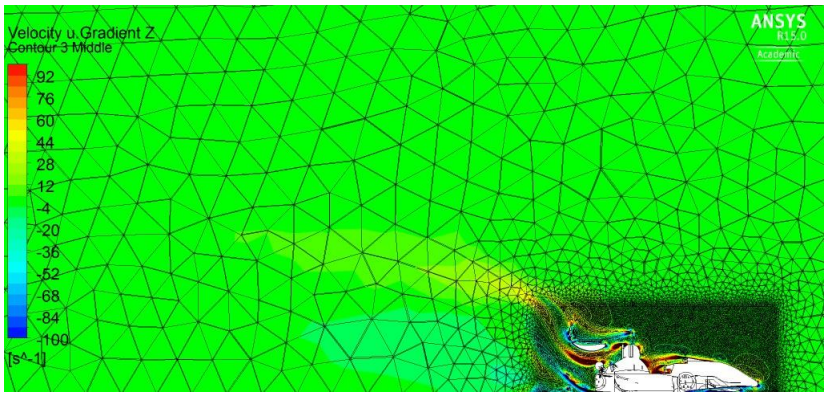

Figure 34: No Wake region, streamwise velocity (∂u/∂z) at planes in ZX at Y=0.

The wake was investigated using smoke in the wind tunnel. The curvature and direction of the flow is consistent with the CFD results but the strength of the structures could not be determined. There are other factors such as the flow collector influencing the height of the wake which is discussed in section 6. Wind Tunnel.

Figure 35: Wake height streamlines from wind tunnel testing.

Until further studies that can determine the wake region are completed, keeping the original wake box with larger height will be used for future simulations.

3.3.3 Farfield

The area with the largest spatial area and also mesh size is the Farfield. This region is used as a standard practice in industry when modelling vehicle aerodynamics and other external aerodynamic applications.

Changing the width of the walls had a minimal effect on the forces on the car but large effect on the momentum at the wall that bounded the Farfield. For a smaller width Farfield, the momentum at the wall doubled the magnitude of momentum and therefore leads to a slight increase in pressure on the wall. By increasing the wall size only slightly reduced this momentum flow. Therefore the width of the Farfield is sufficient for further simulations.

Decreasing the length had an effect on both the wall and roof of the Farfield. Both of these boundaries had an increased in momentum considerably. An extended Farfield was unable to run due to meshing issues which were not determined but due to sensitivities in this direction it is worth investigating this again.

Increasing the height was the most sensitive and effective parameter. Raising the height to double the amount from the baseline is recommended as the momentum was halved without significantly introducing mesh element numbers. Decreasing the height slightly affected the forces as well as increasing the momentum significantly. These results can be found in Appendix 12.6.

3.3.4 Future Domain Setup

From the above studies, it is recommended that future designers use a domain with the dimensions in Figure 36. If the rules are changed again Nearfield width and height and Wake height must be swept through again to determine whether they are the most effective domain sizes before design iterations begin on the design.

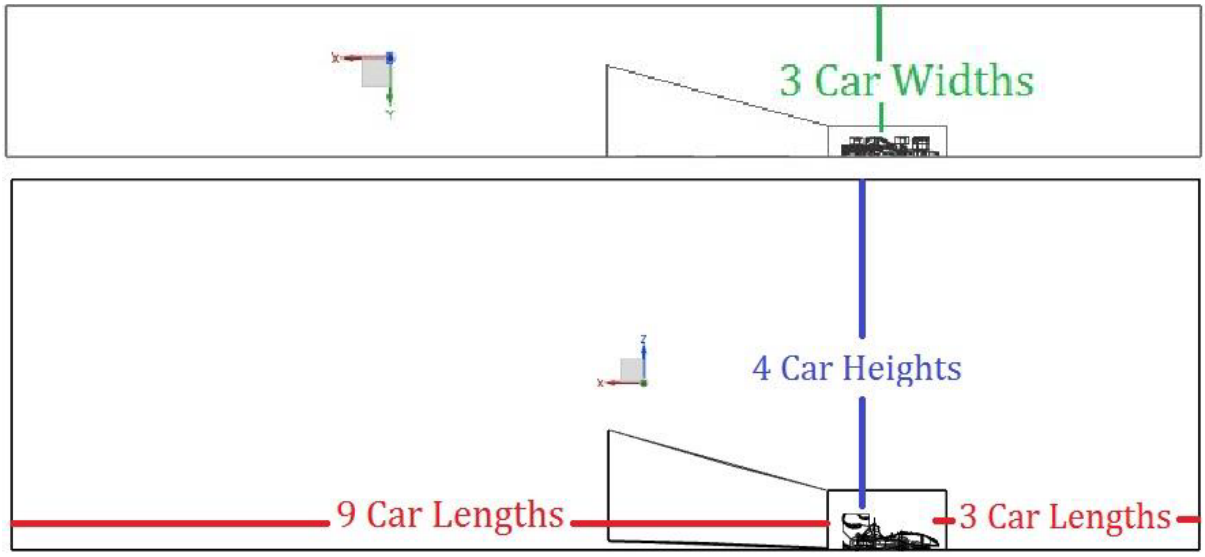

Figure 36: Future Domain Size Setup

3.4 Mesh

3.4.1 Mesh Setup

To ensure the high pressure gradients on the many aerodynamic surfaces the car has, refinement meshes must be created. The following have specific mesh sizing applied to them:

- Front Wing (Face Sizing of 6mm)
- Rear Wing (Face Sizing of 6mm)
- Undertray (Face Sizing of 8mm)
- Bodywork (Face Sizing of 8mm)
- Radiator (Body Sizing of 6mm)
- Near Ground (Face Sizing of 12mm)
- Nearfield (Body Sizing of 30mm)
- Wake (Body Sizing of 30mm)
- Front Wing Refinement Regions (Body Sizing of 30mm)

The number of refinement regions has increased from previous years. This has been driven by more integration between components, especially the nosecone and sidepods.

Growth rate, selected in the sizing options, affects how quickly the mesh grows from the surface to its maximum size. The growth rate for all simulations is set at 1.25. This applies to both the face sizing and body sizing selections.

An aspect of body sizing that hasn't been looked at is the effect of using geometry to determine the mesh as a body of influence. This could be incorporated into the Farfield as it currently consists of tetrahedral elements and a new field drawn from near the start of the Near Field and incorporate the Nearfield and Wake (Figure 37). The hypothesis is that it will create a structured mesh in the Farfield region as the Newfield will enable the transition area required to patch conform. This will be determined in future studies.

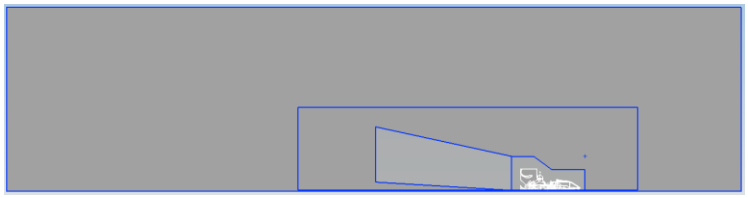

Figure 37: Body of Influence mesh setup.

The inflation layer, required at surfaces that require the no-slip condition, captures the high pressure gradients (zero velocity at surface into high free stream velocity). From Figure 38 below shows that the difference between a favorable pressure gradient (high value without separation) and adverse pressure gradient (separated flow) is considerable and therefore the inflation layer must be refined in order to capture these types of flows.

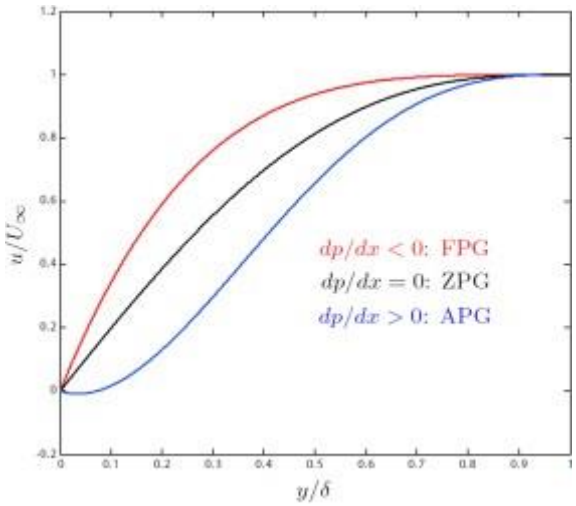

Figure 38: Near wall velocity profile with non-dimensional velocity and distance from wall. FPG = Favorable pressure gradient, APG average pressure gradient and ZPG is zero pressure gradient (LEAP Australia, 2012).

The inflation layer is currently applied to:

- Front Wing and Rear Wing
- Undertray
- Bodywork & Nosecone
- Near Ground and Far Ground
- Wheels and Blends

An example of this inflation being applied to the undertray, shown with the jacking bar and Near Ground, is below in Figure 39.

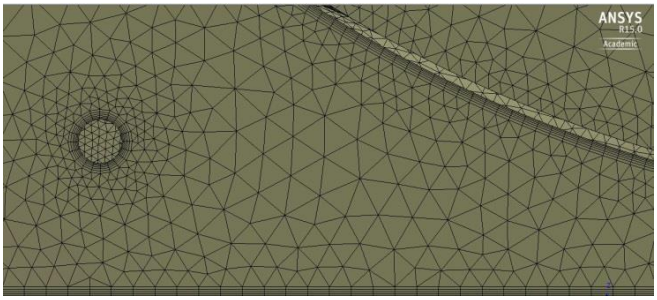

Figure 39: Inflation layers applied to the undertray and jacking bar, viewed from the y axis.

3.4.2 Future Work

The mesh refinement studies that had been planned for this project were unable to be run due to time constraints. However, they will be completed and attached in an addendum to this report. These studies include:

- Inflation layer and Y+ plus correlation and their effectiveness
- Mesh convergence
- Body of influence using Nearfield and Wake
- The 'mid-field' run
- Growth rates

3.5 Boundary Conditions and Expressions

The final setup process before solving a simulation involves setting the boundary conditions in the model (Figure 40). Ensuring the correct turbulence models, inlet and outlet conditions as well as symmetry of the model are selected is integral to the success of the simulation.

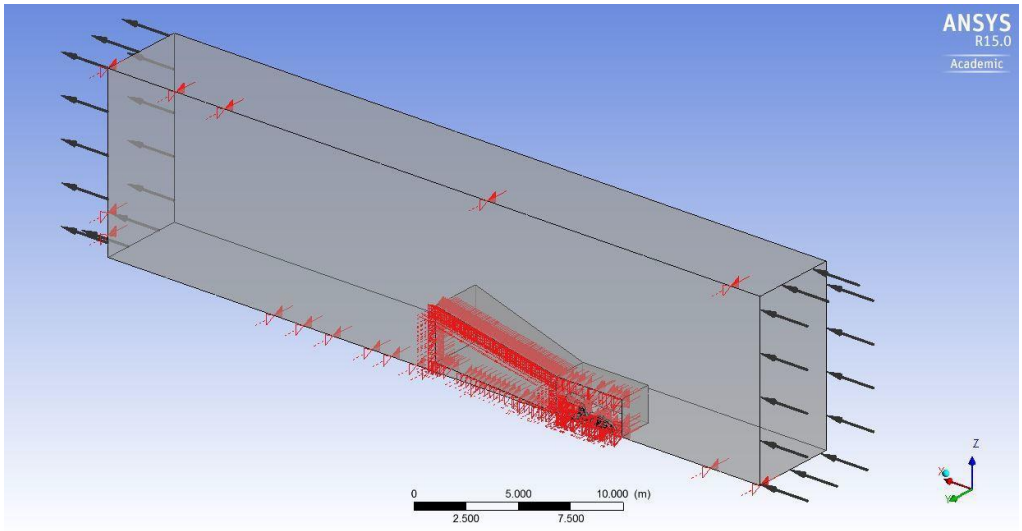

Figure 40: CFX-Pre boundary conditions.

All aerodynamic components and car surfaces (excluding the radiator and intercooler) must be set with a wall condition to notify the solver that it is an impenetrable surface. These components need to be selected into a Named Selection in CFX-Mesh before being selected for wall conditions.

The inlet is then set with the desired speed, chosen as 16.67 m/s, along with the Near Ground and Far Ground that are set as a no-slip wall with a velocity in the u direction as 16.67 m/s. These combine with the outlet which is set to zero average static pressure.

Using wheel speed sensors or theoretical calculation the designer can obtain the wheel speed that is entered as a no slip boundary condition. The wall velocity option allows the user to set the rotation point and velocity in revolutions per second, which for the symmetrical simulations is set at -11.4157 rev/s and parallel to the y axis at a height of 222.41 mm.

To determine the radiator porosity and loss coefficients, wind tunnel testing was completed. Once these values were obtained, the radiator can be modelled as a porous loss model. The streamwise direction is calculated from CAD though currently the radiator is sitting perpendicular to the X axis; therefore it is a loss in the X axis. Permeability, in m^2, and the resistance loss coefficient, in 1/m, from the wind tunnel data are calculated and entered into the boundary conditions. This same process is also applied to the intercooler.

To monitor the force residuals whilst solving and allow for ease of post-processing, expressions are defined in CFX-Pre. The main equations involve the lift and drag forces acting on the major aerodynamic components. Coefficient of lift, drag and pressure are set in the equation set below;

$$C_L = \frac{2 * L}{\rho * v^2 * A} \dots (Eq.\ 2)$$

$$C_D = \frac{2 * D}{\rho * v^2 * A} \ldots (Eq. 3)$$

$$C_p = 2 * \frac{p - p^{\infty}}{\rho_{\infty} * v_{\infty}{}^2} \ldots (Eq. 4)$$

To determine the balance of the aerodynamic loads, both front and rear downforce must be calculated. The location of the origin is in between the front wheels, so the moment about this point must be determined before solving the equations;

$$Rear\ Downforce = \frac{M_Y}{Wheelbase} \ldots (Eq. 5)$$

$$Front\ Downforce = L - \frac{M_Y}{Wheelbase} \ldots (Eq. 6)$$

$$Balance\ (\%) = 100 - \frac{Rear\ Downforce}{Total\ Downforce} * 100 \ldots (Eq. 7)$$

The convergence criteria are set to a root-mean-square (RMS) residual type target. In each control volume, the residual target measures the accuracy of the constant variables. This residual target is $1x10^{-5}$, though this is rarely achieved and the user should continue to use the force residuals to best determine whether the solution has resolved. As mentioned in 3.1.1, the solution should be completed after 300 iterations with a minimum of 250 iterations as the lower limit.

3.6 Model Simplification

Balancing complexity of the CFD model with simplified geometry to allow for reliable meshing is complicated by the constant changing design of the chassis and suspension geometry during the early stages of the design period. Several hours are spent on each new baseline CAD model after new suspension and chassis designs are completed.

In order to simplify and reduce time spent on the new baselines, standard components were designed for the driver, cockpit, steering wheel, engine bay and suspension detail that can be transferred to different designs as these are kept constant throughout the team design period. The changes in design can be seen in Figure 41.

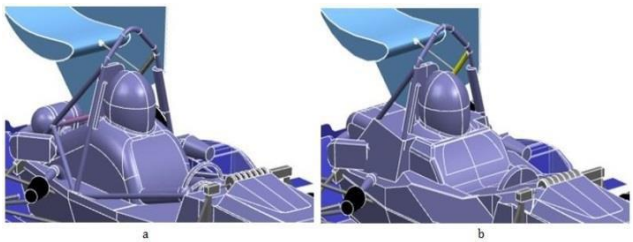

Figure 41: Changes in the driver, cockpit, steering wheel, engine bay and suspension detail. The left picture is the baseline and right is the simplified geometry model.

The benefit of simplifying the geometry is an increase in mesh quality and a reduction in the total number of elements required for a simulation. A total of $6x10^5$ elements were saved from the geometry changes which equates to a reduction of 4% solving time.

The flow structures and forces acting on the car from aerodynamic load were similar for all compared simulations of baseline geometry and simplified geometry. The result was a difference of less than 0.3% for both CL.A and CD.A, with the body and rear wheels contributing the majority of this discrepancy. The pressure in the cockpit is lower than the baseline due to filled out cockpit, and hence reduces the effectiveness of the vortex formed from the cockpit. This weaker vortex doesn't pull flow over towards the dive-plates on the bodywork and results in less downforce being produced.

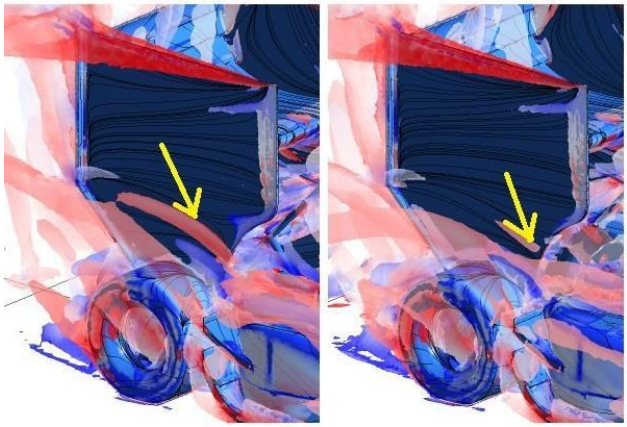

Figure 42: The strong vortex (red rotating outboard and blue inboard) that is formed from the cockpit in baseline, shown on the left, is weaker in the simplified simulation, shown on the right, due to lower pressure gradients between bodywork region and cockpit.

4. ASYMMETRIC MODEL

A variety of yaw angle are seen when the car is navigating a track. To determine what yaw angles both the front and rear wing experiences, cobra probes were attached to both wings and angles were recorded over two different tracks, shown in Figure 43 (Russouw, 2014).

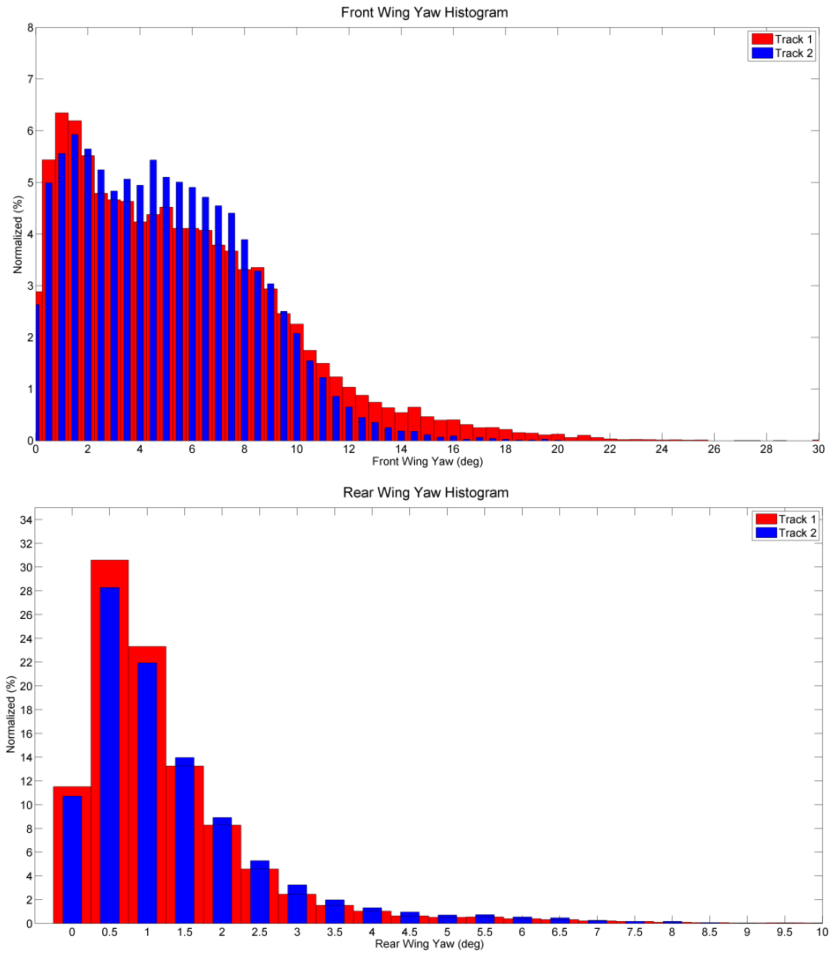

Figure 43: Front (top) and Rear (bottom) wing yaw histograms.

It can be seen that the front and rear wings have different yaw angles across the track. Another interesting aspect is that in both cases, zero degrees of yaw in which symmetrical runs are conducted is not the most common yaw angle. This provides error compared to what would be seen on track.

Simulating the car in the symmetrical CFD model setup provides more errors by the physical car not being symmetrical. The parts that aren't symmetrical about the X-axis are:

- Radiator
- Exhaust
- Intercooler
- Drag Link
- Intake

- Bodywork internal geometry

The other issue of modelling a symmetric model is that the wind tunnel simulation correlation is hindered without the ability to yaw the car to validate components that were added on during the wind tunnel sessions.

In order to investigate the effect these asymmetric geometries have and correlate with wind tunnel data and rotating reference frame, an asymmetric model was created and setup. The car model is shown below in Figure 44.

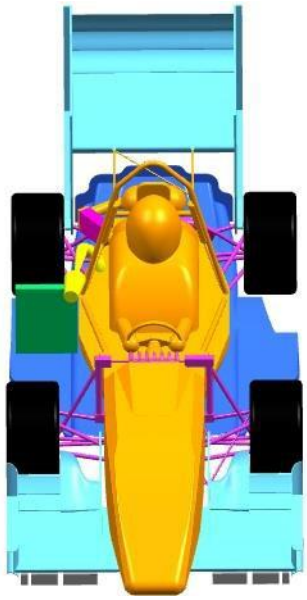

Figure 44: Asymmetric model, notice the pink intercooler radiator in green.

The model has the components such as the radiator located on their correct side of the car but the exception being the exhaust and bodywork internals. These were chosen not to be modelled due to the exhaust being different to CAD and changed to pass noise tests rather than straight from CAD and the extra time required to setup the bodywork on each side with new internals. The slow velocity of the flow and hence low pressure gradient suggested that it would not affect the flow considerably enough to overcome the other issues.

To enable the designers to quickly rotate the car for yaw studies, the Nearfield, Wake region and Farfield were all increased in width as with increased frontal area and flow having a larger influence on the y axis direction of the free stream. The studies from 3.3 are consistent with this theory.

The yaw angle data will be used to determine the yaw angles tested. The maximum yaw angle is 15 degrees though this can be higher for design event data as certain cases, such as wind sensitivities and spinning car, will have much larger yaw angles. These will have to be extreme cases as FIGURE shows the relatively high chance of high speed wind and the chances of the car spinning at high speed is also another rare occurrence.

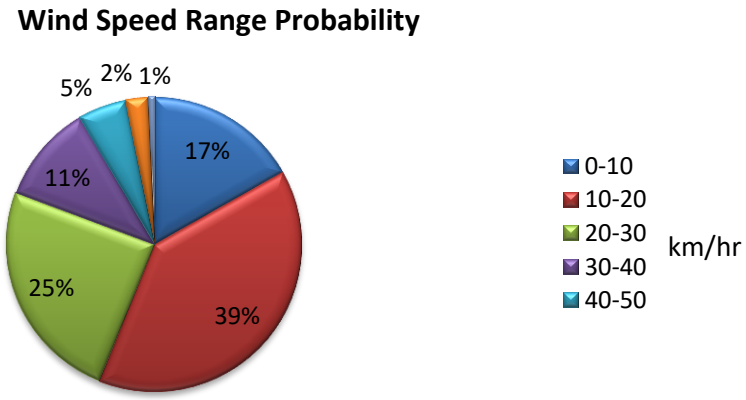

Figure 45: Wind speed and direction at Calder Park (Phersson 2009).

The computational power required for this simulation to complete was approximately 45 GB of memory. This currently can only be solved on the single super-computer located in the Monash Engineering Computer Labs. Therefore these simulations are to be used during the design period once the car concept and other sections have completed their designs as a way to improve the yaw acceptance of the endplates and strakes.

The total mesh element count is nearly 43 million elements. Due to the high number, it isn't worth the time resources to reduce the element count as the simulation will be running for over 30 hours. The designer will have to set-up the simulation and ensure that backup files are created at every 25 iterations so that runs are not left unattended and not solving.

The current model is setup but there are issues in access to the super computer, such as being left unattended for over 24 hours, and issues in the solver to which will be investigated when semester is completed and students no longer require access to the computer.

5. ROTATING REFERENCE FRAME (RRF)

5.1 Motivation

Due to F-SAE rules and safety concerns, competition tracks are designed to an "average speed of 40 to 48 km/hr" (SAE International, 2014). This is achieved by numerous dynamic maneuvers such as chicanes, slaloms and hairpin corners. Data from numerous events showed the car spends 83% of the lap in various types of cornering and is represented below in Figure 46 (Juric, 2008).

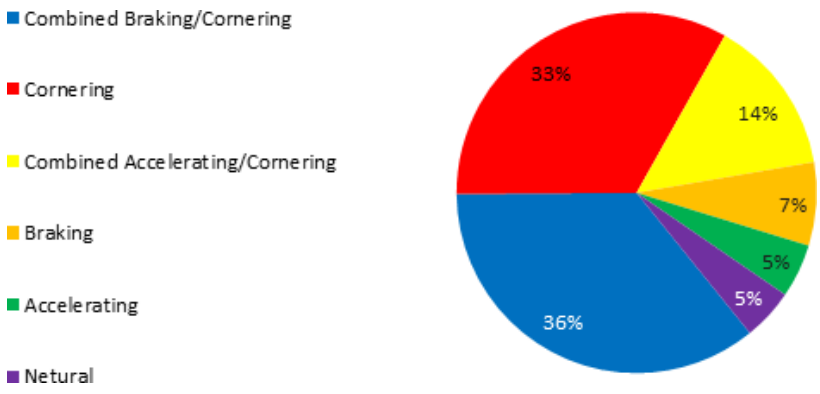

Figure 46: Different modes of driving the car experience throughout a lap. A total of 83% is in some form of cornering/ (Juric, 2008)

To ensure the aerodynamic package has a high performance during these maneuvers, a rotating reference frame CFD simulation was developed (Buckingham, 2012). This simulation used a non-inertial frame of reference that allowed the flow to change direction in the way the car would see if it was making a steady state corner. A setup diagram, Figure 47, shows the relative freestream velocity that is curved and that the front and rear wings see different incidence angles from this curvature.

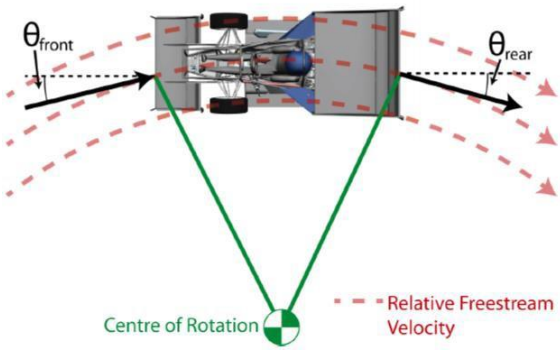

Figure 47: Rotating reference frame and relation to incidence angles (Buckingham, 2012)

The incidence angle was measured using cobra probes and is shown in Figure 48 (Russouw, 2014). The graph shows that the rear wing isn't sensitive to corner radius where-as the front wing has an exponential relationship with the incidence angle and corner radius. As the Skidpad event is within the high gradient section of the exponential relationship, it will be interesting to determine the

effect of different lines taken during the steady state loop and how this affects the downforce. If this indeed does effect the downforce, designers can consider the option of adjustable turning vanes, strakes or endplates for different events.

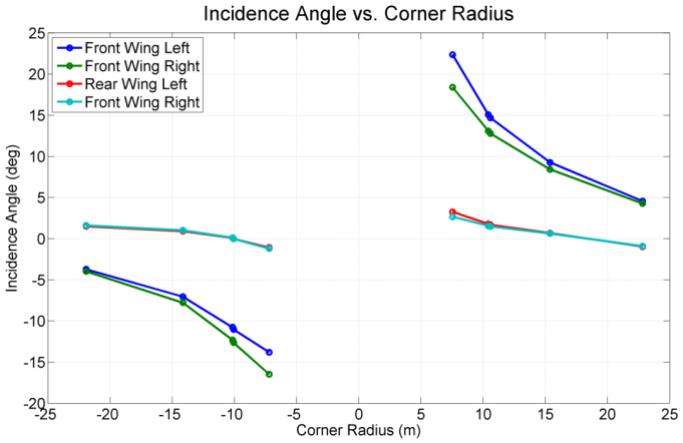

Figure 48: Cobra probe data showing incidence angles of both front and rear wings.

5.2 Additions to the Navier Stokes Equations

From the straight line simulation, two inertial (fictitious) force equations are required to be added to the Navier Stokes Equations. These are the Centrifugal (Equation 8) and Coriolis (Equation 9) (Blazek, 2005):

$$F_{Coriolis} = -2 * (\vec{\omega} \times \vec{\vec{v}_r}) * mass \dots (Eq.\ 8)$$

$$F_{Centrifugal} = -\vec{\omega} \times (\vec{\omega} \times r) * mass \dots (Eq.\ 9)$$

The Coriolis Effect is the deflection in path when viewed from different reference co-ordinates. For this particular rotating reference frame, the air will experience a centrifugal acceleration which will act in a radial outward force. It could also be said that the air will want to travel from the high pressure and slower moving velocity at the inside of the domain straight to the outside of the domain. The Coriolis Effect will move the air to have a curved path (curved the opposite direction to the free stream velocity, to the left in Figure 47) as it gives a force perpendicular to the rotation axis.

The Rossby number, Ro, determines the ratio of inertial forces to the forces from the effects of Coriolis Effect.

$$Ro = \frac{U}{2 * l * \omega} \dots (Eq.\ 10)$$

For a Skidpad domain setup, the Rossby number is 3.2. Any value that is much less than 1 is considered influenced highly by Coriolis forces, above this inertial forces are dominant. The effect this has on the forces and flow structures is insignificant.

5.3 Model Setup

To incorporate this type of simulation into the design period, a CFD model and calculation spreadsheet was developed to allow for all future designers of the aerodynamic package to easily simulate their designs for various cornering radii and speeds.

From the calculation spreadsheet, users can select the type of corner they want to simulate from the Formula Student Germany track. This outputs the corner radius, corresponding theoretical wheel speed and the steered angle of the wheels. The user can then input these values into the new rotating reference frame CAD model and simulation setup.

$$Theoretical\ Wheel\ Speed = \frac{Corner\ Speed * Wheel\ Distance\ to\ Centre}{2\,\pi * Wheel\ Radius * Corner\ Radius}\ \frac{rev}{s} \ldots (Eq.\ 11\ )$$

Since the last data is from FSG in 2014 that has only the first eight laps from endurance worth of data, the wheel speed is consistent with theoretical numbers. An example of the wheel speed outputs in shown in TABLE and an example of the spreadsheet is given in Appendix 12.7

Table 2: Wheel speed (rev/s) for varying types of corners (FL=Front Left, FR = Front Right, RL = Rear Left, RR = Rear Right).

Corner	FL	FR	RL	RR
Aus Skidpad	7.908	9.025	8.086	9.137
FSG Sweeper	10.988	11.690	11.047	11.717
FSG Cone Killer	12.306	12.966	12.355	12.985
FSG Slalom	10.739	11.512	10.810	11.547
FSG HW Hairpin	6.797	7.840	6.975	7.954
FSG Pendulum	15.472	15.982	15.499	15.988

The resultant forces and moments on the car are required for post processing. Figure 49 below shows the spatial co-ordinates, X-Y-Z, and their corresponding Roll-Pitch-Yaw moments.

Figure 49: X (red) –Y (green) - Z (blue) and Roll (pink) –Pitch (light green)-Yaw (light blue)

The moments can be calculated using CFX-Post using the following expressions (selecting "torque_y_'axis'()" on all components):

$$Roll = M_X@Centre\ of\ Gravity \ldots (Eq.\ 12)$$

$$Pitch = M_Y@Centre\ of\ Gravity \ldots (Eq.\ 13)$$

$$Yaw = M_Z@Centre\ of\ Gravity \ldots (Eq.\ 14)$$

5.4 Future Work

More studies are to be completed before FSAE-Australasia to further investigate the effect incidence angle has on flow structures and forces acting on the car.

To enable future designers conduct RRF, a tutorial will be completed on how to setup the domain and how to use the spreadsheet to enter the data. By having more designers able to conduct this simulation, the larger chance more of these simulations being used and therefore the potential benefit of designing for yaw cases.

There is potential with the RRF calculation spreadsheet data to run multiple simulations at varying corner radii and speed. Using this data, one could use the change in CL.A and input this with a lap-time simulator created by Bett, 2015. This will allow the designer to see whether the large incidence angles seen for small radius corners are worth designing for and the same goes for straight line simulations if there is a large difference at low incidence angles.

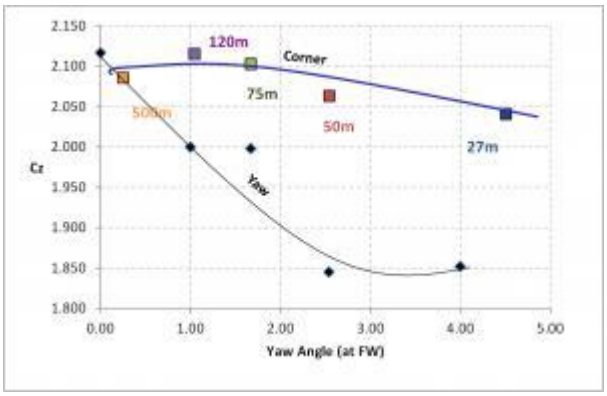

Figure 50: Coefficient of lift at varying corner radii and yaw angles (Total Simulation, 2008)

6. WIND TUNNEL TESTING

Monash Motorsport is fortunate to have access to in Monash University's 1.4MW open-jet wind tunnel for approximately a week each year. Numerous studies into external aerodynamics, such as symmetrical car models and radiator specific dissipation, have been completed over the years to gain an understanding of how to both improve and validate the car.

Testing the F-SAE car in a wind tunnel without a moving ground provides errors in flow structures and aerodynamic load on the car, as the components rely on ground effect.

6.1 Ground Boundary Layer

To bring the testing closer to simulation the car needs to be elevated above the boundary layer growing on the test section floor (Katz, 1995). This boundary layer, without elevation above it, will have larger errors compared to on-track and CFD as it will have zero velocity under the front wing and undertray. Katz suggests other methods of removing this boundary layer but all are unavailable to implement in the wind tunnel or are too time and human resource expensive.

The boundary layer thickness can be determined by the data provided from the Monash Wind Tunnel as the effect of the inlet contracting to reduce its thickness is difficult to theorize. An approximate assumption can be made using the turbulent boundary layer thickness equations (Cengel & Cimbala, 2006):

$$\delta = \frac{0.385 \cdot l}{{Re_x}^{0.2}} \ldots (Eq. 15)$$

$$Re_x = \frac{\rho \cdot u_0 \cdot l}{\mu} \ldots (Eq. 16)$$

6.2 Tunnel Testing Rig and Groundplane

To elevate the car and also span across to the Kistlers (force sensors) a new Tunnel Testing Rig (TTR) was designed and constructed. Using 100x50x3mm RHS steel as the main structure of the TTR means there is minimal deflection when under aerodynamic loading, car mass and multiple designers standing on it. The Kistler dimensions were based off an old Suzuki car model as this was the closest to Monash's wheelbase and track width. CAD and final construction of the rig is shown in Figure 51.

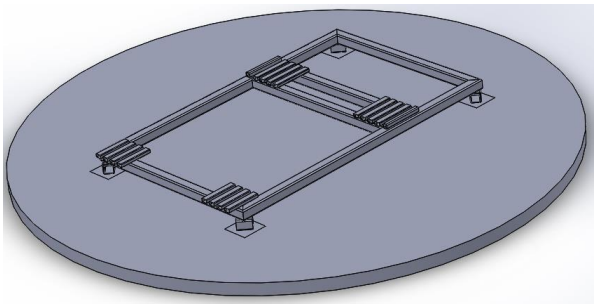

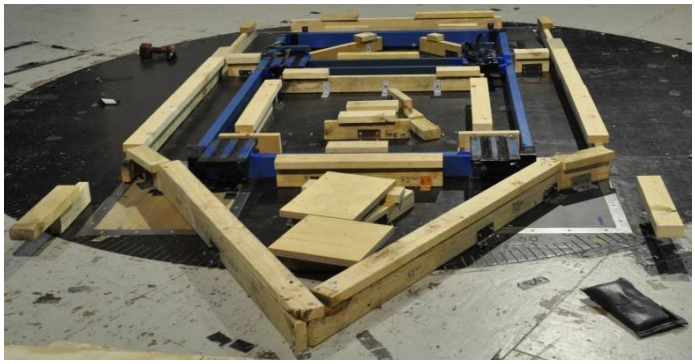

Figure 51: CAD model of the TTR (top) and groundplane mounting with TTR in the wind tunnel

With an elevated car, an elevated surface to act as the new ground is required. This was achieved by using timber to support a plywood surface. This was extended around the entire car to aim for a higher correlation to CFD and on-track. A triangular shape was added underneath the groundplane to divert the ground boundary layer flow around the test section. Long planks were used to roll the car on and off the front of the TTR, which required minimal lifting. This is an improvement over previous years as carrying the car over a thin groundplane was prone to damage the plywood or injure someone. A side view of the groundplane with M15 in secured in position is shown in Figure 52.

Figure 52: M15 on the groundplane.

Improving the groundplane so that it extended around the entire was beneficial in correlating undertray flow. Whilst the errors due to not having a moving ground would be present, smoke visualization of the undertray exit flow on the outside tunnels had similar flow speed and direction, which is promising for the design and correlation.

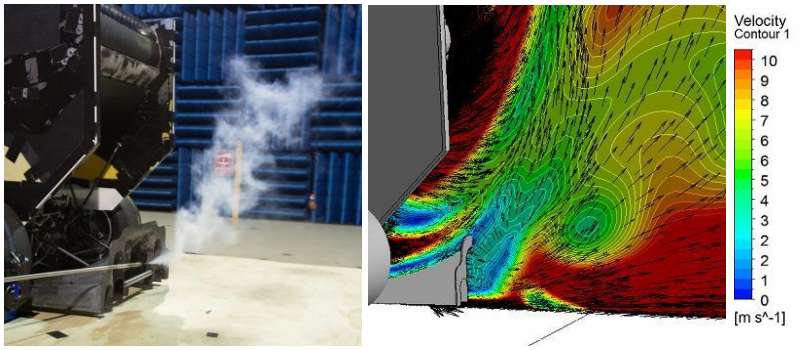

Figure 53: Outboard section flow from undertray in wind tunnel (left) and velocity contour with tangential vectors (right).

6.3 Wheel Tripper

Stationary wheels also provide errors in the model compared to on-track and CFD as it has a separation point further back on the tyre surface at lower Re numbers. This separation is approximately at 160 degrees from the bottom of the wheel on the rear of the tyre. Due to the change in size of the tyres from inconsistent pressures, ensuring the flow over the tyre is correct becomes more critical.

To simulate the drag and flow structures that would be seen on-track and CFD, a small vertical flat plate was fixed to the top of the top of the tyre to 'trip' the flow earlier. This resulted in a separation point that matched the CFD simulations and similar flow structures.

Further improvements to this modelling would be to reduce the size of the flat plate and obtain drag coefficients with and without the wheel tripper.

Figure 54 shows that the stationary wheel with the flow tripper definitely makes a difference and correlates well with Katz's rotating wheel.

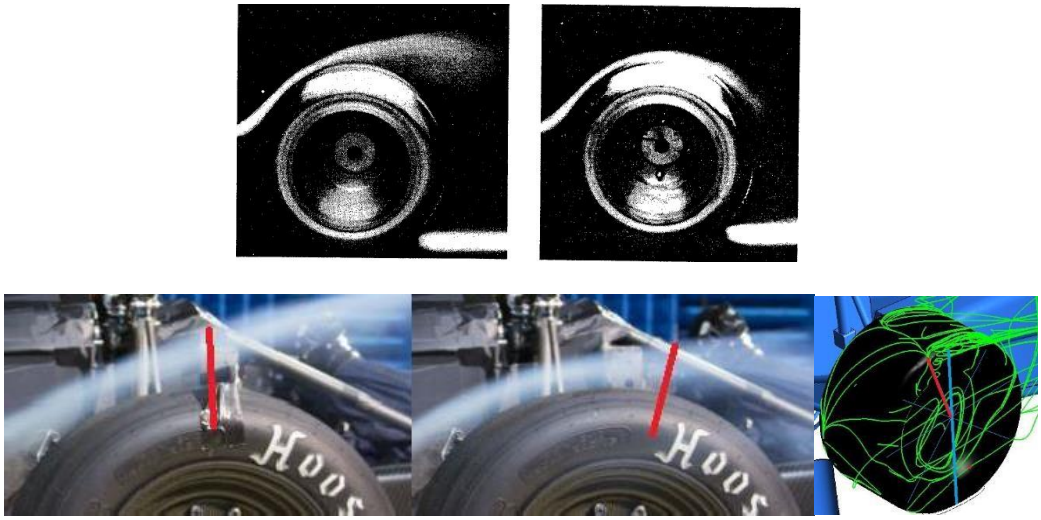

Figure 54: (clockwise from top left) rotating wheel with smoke, stationary wheel with smoke (note the separation point further back on the wheel) (Katz, 1995), CFD constant streamlines with the red line the radial location of the separation, stationary wheel of M15 in the wind tunnel, stationary wheel with flow tripper attached.

6.4 Blockage Effects

The blockage effects from open-jet wind tunnels are minimal (SAE International, 1994) as the frontal area is 2.4% of the testing section size. There is also insignificant effect from the flow collector on the car. Using smoke visualization, the wake from the car was found to be approximately 3m which is 0.5m lower than seen in CFD simulations. This 0.5m region is relatively weak flow structures and hence can be ignored.

6.5 Driver Model & Height

As it is unreasonable for the same person to be sitting in the car for all the tests conducted throughout the week, a driver model was created using an adjustable neck and accurate upper-body figure. Previous models were last minute designs, hence the geometry in FIGURE where tape is wrapped around the main roll hoop and the absence of shoulders. The new geometry used a timber

member to adjust the height so driver head height sensitivity studies could be conducted, hands and arms that were connected to the steering wheel and breadth of shoulders. The difference between an actual driver sitting in the cockpit and the drive model is minimal and with more importance on the flow near the helmet on the performance on the reduced span rear wing is greatly increased.

Figure 55: From left to right: 2013 driver model, 2015 driver model and actual driver in M15.

6.6 Testing Rear Endplates

The restricted and busy testing schedule to improve the setup and reliability of the car has resulted in a restructure of manufacturing and testing processes for the aerodynamics section. On-track testing begins before tunnel testing, so the choice of what components are built for competition and which are built to be modifiable must be determined. Previously, all components were built for competition and plywood endplates were used to conduct wind tunnel testing. Due to the small gains seen from modifying the endplates and other parts of the car, the majority of the findings in the tunnel did not get built for competition.

To fix this issue, fiberglass sandwich panels were constructed that could be both modified and driven on at the same time. This meant the findings from the wind tunnel could be checked in CFD and then the design can be changed for the final competition-spec endplates.

6.7 Flow Visualisation

6.7.1 Wool Tuffs

Wool tuffs allow for visualization of the direction of flow on a surface. By cutting numerous 20mm sections, a considerable amount of the car's surface can be mapped. To increase the effectiveness of this type of visualization in the future, only half span will be covered. This is due to the small differences in most of the component's forces. Clear tape should also be used along with particular points to take a photo from to which can then be lined up to CFD and on-track results.

A method that was new was using a GoPro mounted to the tuff wand. This method allowed users to view the flow structures found by the wand from a close and direct view. This view can be seen in Figure 56.

Figure 56: Tuff wand with GoPro mounted. Excellent video footage was seen from this new technique.

6.7.2 Smoke

Smoke was generated and swept across the car. Whilst the speed the smoke is generated at is slow, the Reynolds number is only slightly lower than the Reynolds number at the mean speed.

The main benefit of smoke is determining certain flow structures, such as the 3d profile on the front wing or the outer endplate in the Figure 57 below, to see if they can be manipulated and improve the performance of the car.

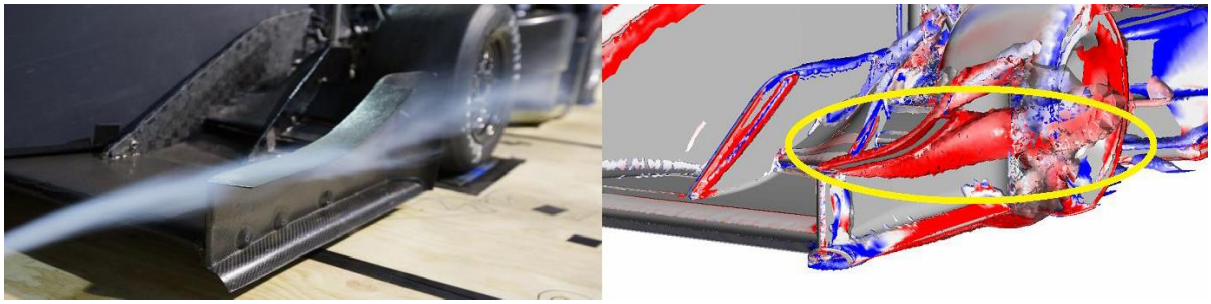

Figure 57: Use of smoke to visualize vortex forming off the side of the front endplates, correlates well with CFD simulation.

6.7.3 Surface Streamlines

One of the more common methods done on the team is the use of an oil-based fluid with an early flash-off point. This allows the driver to complete approximately 10 laps of straight line testing before it dries. They are a variety of recipes for the mixture and therefore changes depending what are available. Monash Wind Tunnel's flow-vis is currently the best mixture available for Monash Motorsport. To best capture the streamlines and be able to compare to CFD, UV lights are used in a dark room.

This test can be correlated with the surface streamlines from on-track testing. An example of surface streamlines and CFD streamlines can be seen in Figure 58.

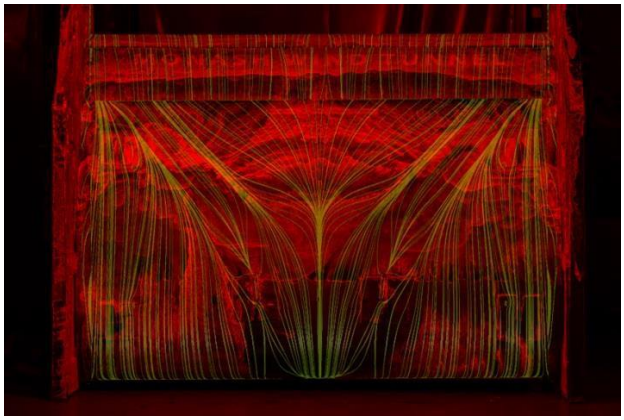

Figure 58: Surface streamlines from oil-based mixture (red) overlaid with CFD streamlines (green).

6.8 Future Work

To further improve the wind tunnel model, investigation into sucking the boundary layer through the start of the ground plane would be better method of removing it whilst not being overly resource expensive.

Numerous studies were conducted in the wind tunnel and therefore validating these in a wind tunnel CFD simulation would provide greater insight into the errors and drawbacks that it has. This will be achieved by keeping the same domain but raising the ground to the same height as the wind tunnel test model and having no moving ground. The only issue with this is aiming for a similar boundary layer off the ground and whether this correlates with the wind tunnel.

Pressure tapping the wings in the wind tunnel is also an aim for 2015, as the wings are currently constructed and require only a day of testing allocation. Due to the tight schedule in the lead-up competition, it is possible it could happen in before the team travels to Europe in mid-2016.

7. ON-TRACK TESTING

7.1 Pressure Tapping

Pressure tapped wings were created for M15 to be used in both wind tunnel testing and on-track testing (Figure 59). Due to time constraints, from extended manufacturing time and the wind tunnel staff unable to get the DPMS software running, pressure tapping was withheld till either before competition in Australia or before Europe in mid-2016.

Figure 59: Rear (top) and front (bottom) mainplanes that have been pressure tapped and with all mounting attached. Requires the use of DPMS unit before testing.

A total of 22 taps are expected to be available for each wing. Since there is only a small amount of pressure taps and the concern for frequency response of the pressure tapping lines, the rear wing pressure transducer will be located inside the wing itself whilst the front wing pressure transducer will be located in front of the pedal box.

The location of these pressure taps had to be placed to ensure the best data can be obtained from the tests. Therefore, the lowest pressure regions were focused on as well as the leading edge, shown in Figure 60.

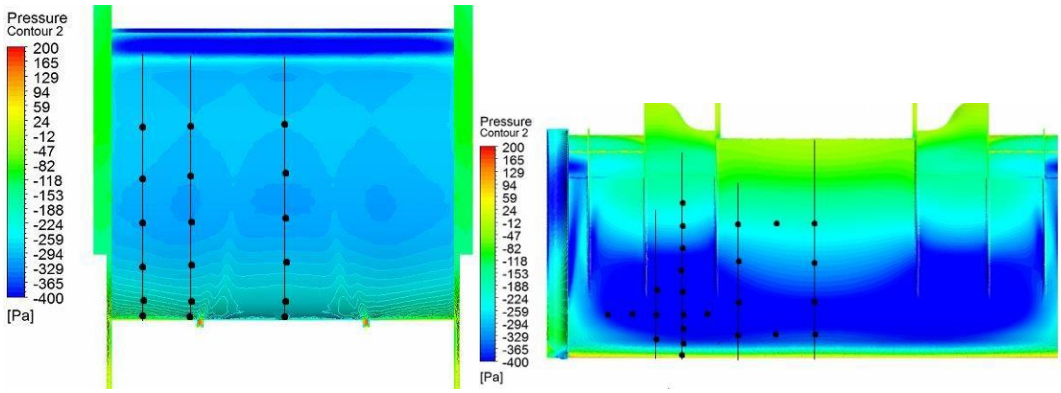

Figure 60: Rear (left) and Front (right) mainplane pressure contours. The black dots represent the locations of where the pressure will be measured.

7.2 Physical & Quantitative Data

Coefficient of Lift has an inverse square relationship with velocity. By doing different radii in steady state conditions, theoretically there should be an inverse square relationship with the coefficient of friction of the tyres. Previous testing of this has shown a constant gain of 5km/hr for constant radius sizes past 12m which covers the majority of corner radii.

To determine the drag coefficient, coast down runs were completed at the Australian Automotive Research Centre. This involves reaching approximately 80 km/hr and then rolling for as long as possible. This is then repeated in both directions. The data obtained from this test was inconclusive and further tests will be undertaken to further validate the car's drag coefficient.

A thesis was completed on strain gauging suspension components (Salvo, 2014). The comparison of tyre lateral force to tyre normal force correlated with expected trends but quantifying whether this improves the performance and changes the tyre behavior was not determined. Extending this into vehicle yaw response and strain gauging the wing mounts there is potential to see how the aerodynamic load varies through different corners.

Using cobra probes, a four probe pitot tube that determines the air velocity the designers can find the incidence angle. This was done and plotted, shown in section 4 – Asymmetric.

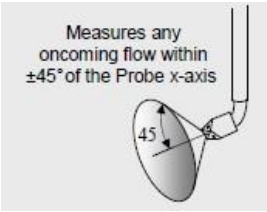

Figure 61: Cobra Probe functions

7.3 Future Work and Concepts

In order to plot large regions of pressure, mounting a wake rake to the car and measuring this across different cornering maneuvers would give excellent correlation with RRF CFD and also symmetrical CFD. This has been done in the wind tunnel recently but it is something the team will have to build themselves due to the high risk when mounting the wake rake to the car, borrowed equipment should not be used.

A simpler but more qualitative method is using fishing wire in a grid fashion and then gluing wool tuffs across this grid. Filming this with GoPro's/small cameras to see how the major flow structures behave during these transient cases.

The third concept is to use smoke machines or generators to which the car then drives through. The benefits being that major flow structures can be verified on-track, and minor structures with careful camera placement and lighting can be verified too.

8. CONCLUSIONS

This project aimed at improving Monash Motorsport's aerodynamic package design process. To achieve this, quicker solving CFD simulations running in conjunction with highly complex cornering CFD simulations, better wind tunnel modelling and data acquisition and improved on-track testing were looked at.

The project was successful in that a 59% reduction in solve time for the symmetrical straight line simulation from changing the domain size, model simplification and re-evaluating the convergence criteria. Post processing results has been streamlined with quicker state files and a more intuitive and fluent process of documenting the Monash Motorsport's Google Wiki has been implemented. The introduction of a stiffer rig and larger and higher quality ground plane which showed had flow coming through the undertray is a positive step towards correlation.

These successes helped Monash Motorsport design their aerodynamics package with greater confidence in results and allowed for a greater number of designs and investigations to be completed. Further development (pressure tapping, wind tunnel CFD, mesh refinements), most of which being conducted in the summer of 2015, will aid the team going into 2016 and beyond. This further development is required as there will always exist negative aspects to each part of the testing and constant evaluation of the design tools must be completed to ensure that there as many options available to the future designers.

9. ACKNOWLEDGEMENTS

I would like to acknowledge all the guidance and support from Dr. Scott Wordley and Damien McArthur plus thank Marc Russouw, Andrew Salvo, Martin Bett, Terence Avadiar, Nathan Humphrey, Thomas Knast, Cameron Warne and Matthew Bartlett for their advice on aerodynamics and suspension.

I would also like to thank:

- The entire aerodynamics section that has worked tirelessly to produce the M15 aerodynamic package.
- The entire Monash Motorsport team, from previous years and 2015, for producing outstanding cars to work on.
- The Monash Wind Tunnel staff for help and supervision during wind tunnel testing
- Bosch Australia for use of testing facilities at the Australian Automotive Research Facility.
- LEAP Australia for their help in understanding computational fluid dynamics.
- My family and friends for their support throughout this project and degree.

10. REFERENCES

Ahmad, Nor; Abo-Serie, E; Gaylard, A. (2010). "*Mesh Optimization For Ground Vehicle Aerodynamics"*. CFD Letters. 2 (1), 54-65.

Blazek, J. (2005). Computational fluid dynamics. Amsterdam: Elsevier.

Bradley Duncan, (2010). "*CFD Approach To Evaluate Wind-Tunnel And Model Setup Effects On Aerodynamic Drag And Lift For Detailed Vehicles"*. SAE International. Stuttgart: SAE International.

Buckingham, S. (2012). "*High Fidelity Computational Analysis Of The Monash Formula SAE Racecar*". Melbourne: Monash University

Cebeci, T. and Cebeci, T. (2004). Analysis of turbulent flows. Amsterdam: Elsevier.

Cengel Y.A, Cimbala J.M. (2006). "*Fluid Mechanics: Fundamentals And Applications"*. New York: McGraw-Hill

Cooper, K. (1993). "*Bluff-Body Aerodynamics As Applied To Vehicles*". Journal of Wind Engineering and Industrial Aerodynamics, 49, pp.1-22.

de Souza, A. (2005). "*How To Understand Computational Fluid Dynamics Jargon*". NAFEMS,1-86.

Hammas, M., Johansson, J. and Skarnell, H. (2010). "*Large Eddy Simulations Of The Flow Around An Ahmed Body With Active Flow Control*". Associate Professor Sinisa Krajnovic. Gothenburg: Chalmers University of Technology.

Juric, P. (2008). "*Design And Manufacture of the 2008 Monash FSAE Suspension*". Melbourne: Monash University.

Katz, J. (1995). "*Race Car Aerodynamics - Designing For Speed*". Cambridge (USA): Bentley Publishers.

Mapson, A. (2011). "*Design, Manufacture And Testing Of Suspension For A Formula SAE Car*". Melbourne: Monash University.

Phersson, L. (2009). "*Formula SAE Aerodynamic Package; Design, Development And Validation*". Final Year Project 2009, p1-77.

Uchida, Okumura, Kuriyama. (1997). "*Aerodynamic Simulations By Using Discontinuous Interface Grid And Solution Adaptive Grid Method*". Society of Automotive Engineers. 970141 (1), 86-89.

.

11. APPENDICES

11.1 Complete Table of Force Standard Deviation

Parts	STD 1000-2000	Δ% 100/200	STD 2000-2500	Δ% 100/250	STD 2500-3000	Δ% 200/300	STD 3000-3500	Δ% 250/350	STD 3500-4000	STD Total Score	Percentage_DF	Average Value	Solved Value	Net Value (Avg - Solved)
Front Wing (FW)	1.01	24.80	1.34	18.66	1.13	36.10	0.83	20.32	1.04	1.09	38.23	229.96	228.93	1.04
FW Mainplane	0.31	20.24	0.38	21.46	0.31	10.92	0.28	7.18	0.31	0.33	11.95	71.89	71.56	0.32
FW Mainplane Flap Section	0.39	39.82	0.65	62.75	0.40	7.32	0.37	10.05	0.42	0.48	16.79	100.98	100.57	0.41
Rear Wing (RW)	1.11	3.69	1.15	51.23	0.76	1.85	0.77	13.55	0.89	1.53	30.86	185.65	184.95	0.70
RW Flap 1	0.16	29.83	0.23	85.80	0.12	19.92	0.16	9.55	0.17	0.31	4.06	24.40	24.30	0.10
RW Mainplane	0.93	1.20	0.92	82.29	0.50	0.15	0.50	41.26	0.86	1.09	26.58	159.92	159.39	0.53
Nosecone	0.21	6.79	0.22	53.95	0.14	16.80	0.17	45.04	0.12	0.21	0.97	-5.85	-5.86	0.00
Intercooler Flow	1.19	65.57	0.72	115.65	0.33	42.26	0.58	24.49	0.76	1.54	11.45	68.88	69.56	-0.68
Radiator Flow	2.60	182.12	0.92	48.28	0.62	9.79	0.57	21.34	0.72	1.99	80.80	486.04	487.58	-1.54
Sidepod Edge	0.26	906.57	0.03	11.47	0.03	47.02	0.02	20.21	0.02	0.22	0.53	3.21	3.36	-0.15
Sidepod Top Surface	0.21	6.42	0.23	11.16	0.21	14.41	0.18	20.53	0.23	0.23	3.51	-21.11	-21.03	-0.08
Sidepod 2	0.37	33.34	0.28	12.48	0.25	12.04	0.22	19.73	0.27	0.32	3.21	-19.30	-19.27	-0.03
Undertray (UT)	1.13	49.18	0.76	4.78	0.72	35.70	1.12	16.81	0.96	1.00	50.32	302.70	303.90	-1.21

UT Inboard Tunnel	0.25	167.38	0.09	2.61	0.10	26.19	0.13	15.86	0.11	0.22	4.03	24.23	24.26	-0.04
UT Outboard Section	0.27	381.48	0.06	30.01	0.08	36.32	0.13	22.68	0.10	0.29	9.75	58.62	58.88	-0.26
Front Downforce	1.66	41.27	2.83	33.31	2.12	15.64	1.83	1.44	1.86	2.65	45.32	272.60	272.29	0.31
RearDownforce	2.29	28.49	3.21	57.98	2.03	21.02	2.57	4.10	2.68	3.76	54.69	329.00	328.85	0.15
TotalDrag	0.96	24.93	1.28	50.92	0.85	23.59	1.11	26.04	0.88	1.70	42.05	252.93	252.14	0.79
TotalDownforce	2.67	358.35	0.58	26.48	0.79	31.03	1.15	3.27	1.11	2.02	100.00	601.55	601.14	0.41
Total	17.99		15.88		11.51		12.70		13.53	20.98				0.77

11.2 Graphs showing force residuals and standard deviation

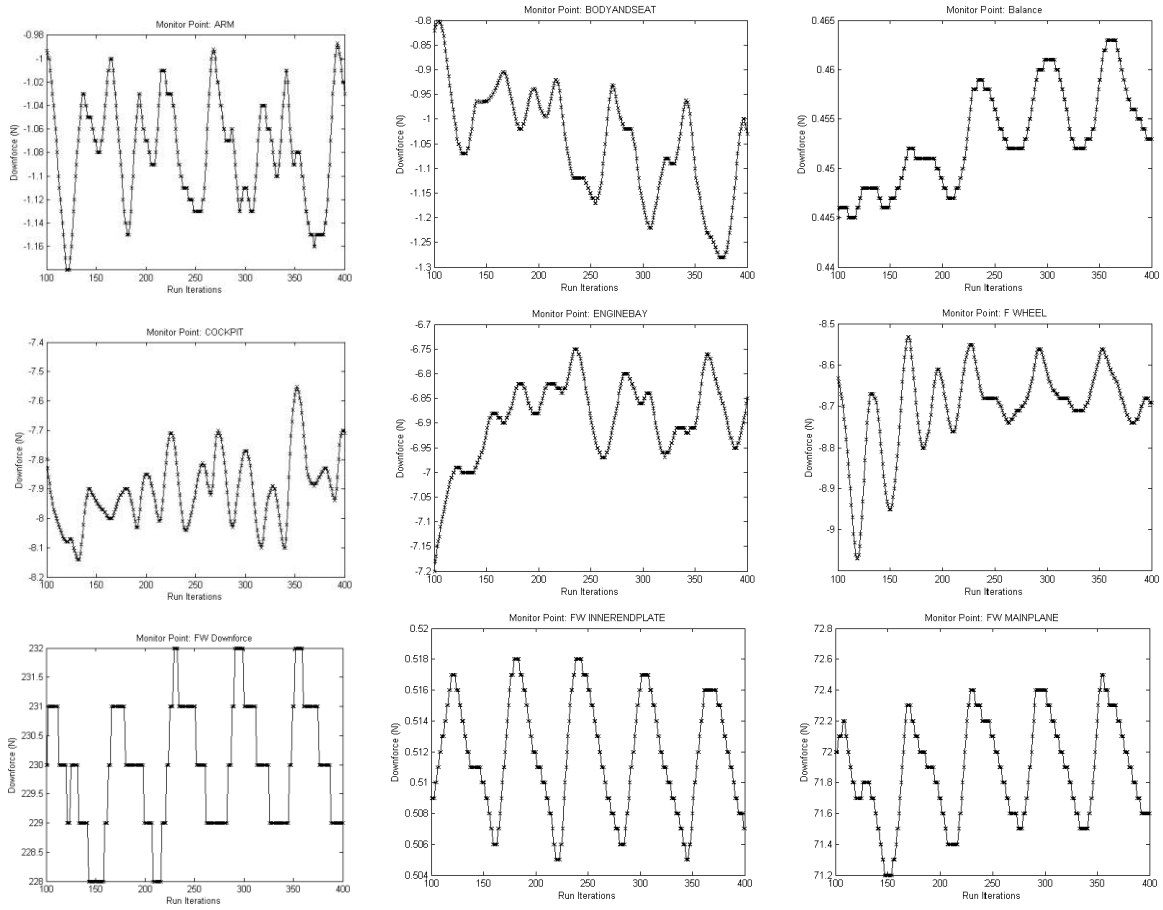

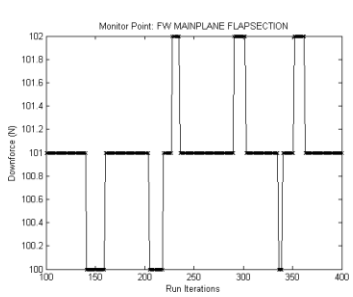
Monitor Point: FW MAINPLANE FLAPSECTION
Downforce (N)
Run Iterations

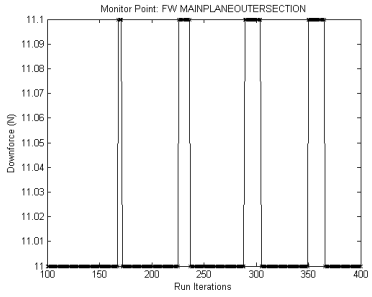
Monitor Point: FW MAINPLANEOUTERSECTION
Downforce (N)
Run Iterations

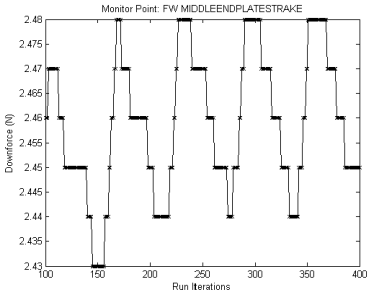
Monitor Point: FW MIDDLEENDPLATESTRAKE
Downforce (N)
Run Iterations

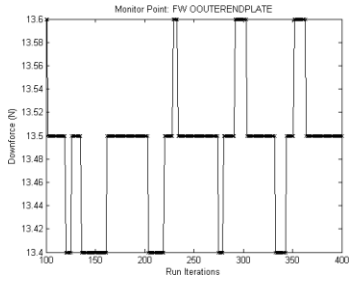
Monitor Point: FW OOUTERENDPLATE
Downforce (N)
Run Iterations

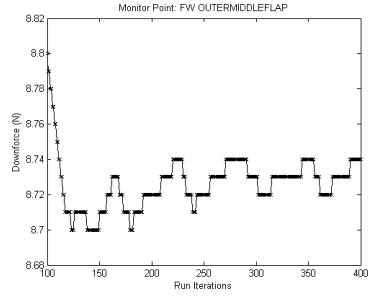
Monitor Point: FW OUTERMIDDLEFLAP
Downforce (N)
Run Iterations

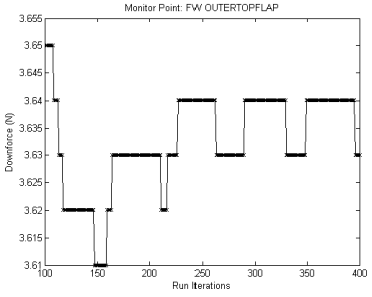
Monitor Point: FW OUTERTOPFLAP
Downforce (N)
Run Iterations

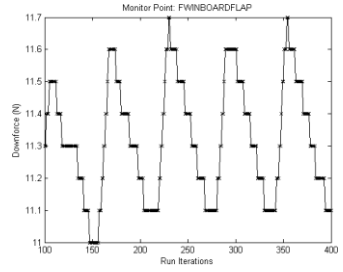
Monitor Point: FWINBOARDFLAP
Downforce (N)
Run Iterations

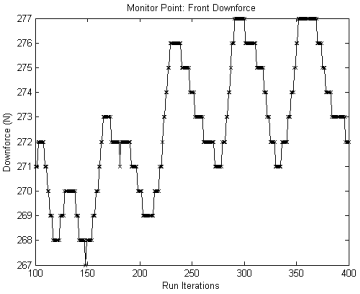
Monitor Point: Front Downforce
Downforce (N)
Run Iterations

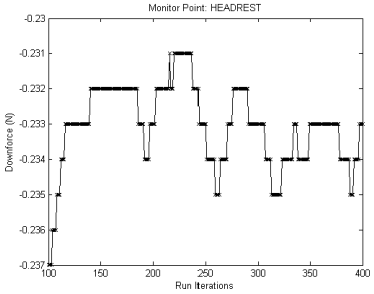
Monitor Point: HEADREST
Downforce (N)
Run Iterations

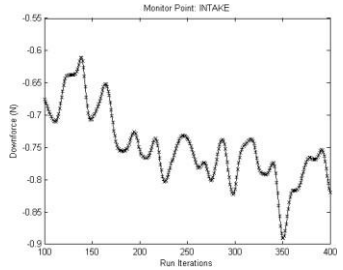
Monitor Point: INTAKE
Downforce (N)
Run Iterations

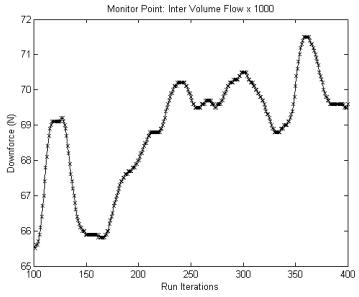
Monitor Point: Inter Volume Flow x 1000
Downforce (N)
Run Iterations

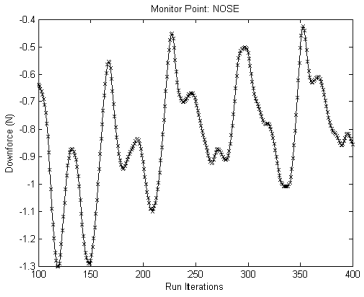
Monitor Point: NOSE
Downforce (N)
Run Iterations

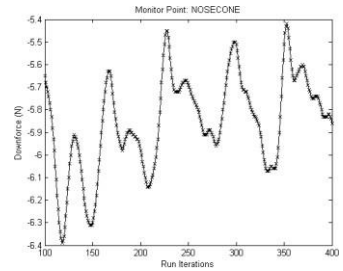
Monitor Point: NOSECONE
Downforce (N)
Run Iterations

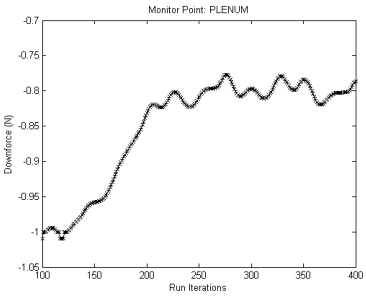
Monitor Point: PLENUM
Downforce (N)
Run Iterations

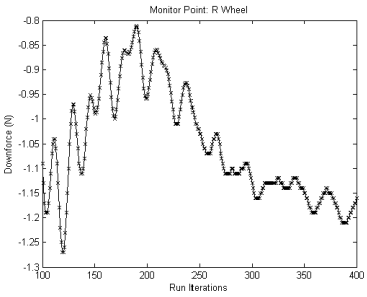
Monitor Point: R Wheel
Downforce (N)
Run Iterations

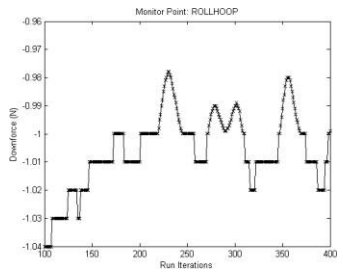
Monitor Point: ROLLHOOP
Downforce (N)
Run Iterations

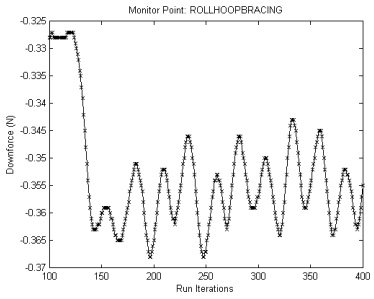
Monitor Point: ROLLHOOPBRACING
Downforce (N)
Run Iterations

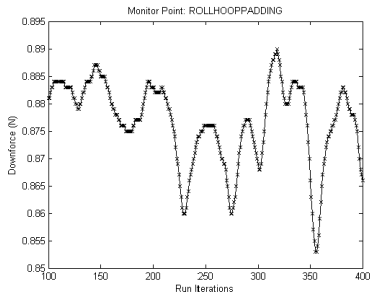
Monitor Point: ROLLHOOPPADDING
Downforce (N)
Run Iterations

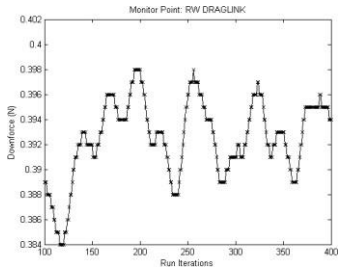
Monitor Point: RW DRAGLINK
Downforce (N)
Run Iterations

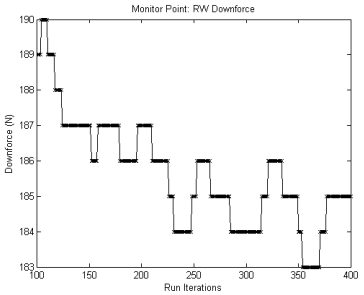
Monitor Point: RW Downforce
Downforce (N)
Run Iterations

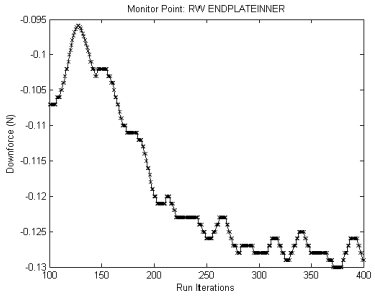
Monitor Point: RW ENDPLATEINNER
Downforce (N)
Run Iterations

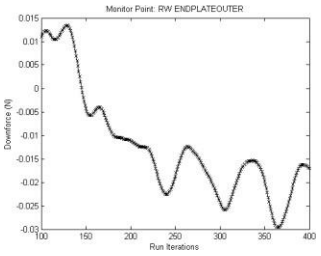
Monitor Point: RW ENDPLATEOUTER
Downforce (N)
Run Iterations

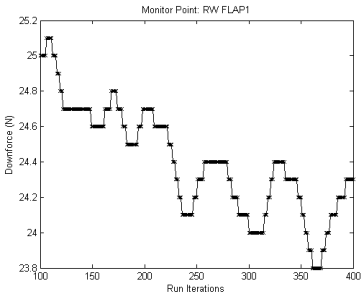
Monitor Point: RW FLAP1
Downforce (N)
Run Iterations

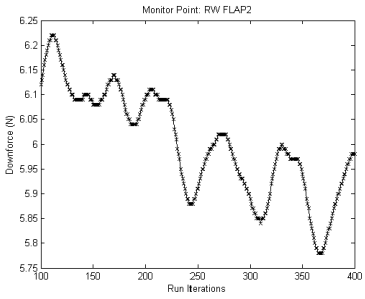
Monitor Point: RW FLAP2
Downforce (N)
Run Iterations

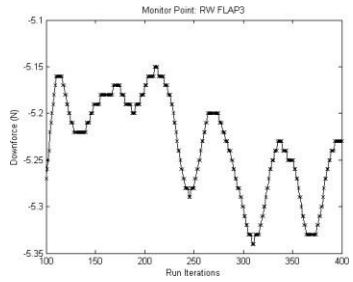
Monitor Point: RW FLAP3
Downforce (N)
Run Iterations

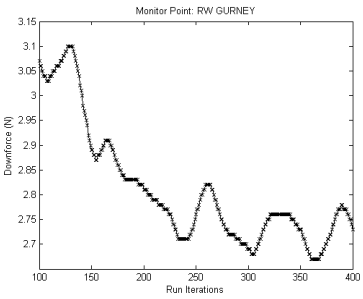
Monitor Point: RW GURNEY
Downforce (N)
Run Iterations

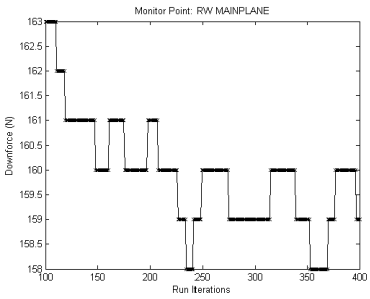
Monitor Point: RW MAINPLANE
Downforce (N)
Run Iterations

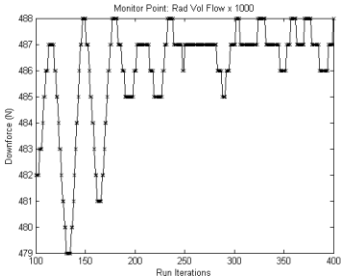
Monitor Point: Rad Vol Flow x 1000
Downforce (N)
Run Iterations

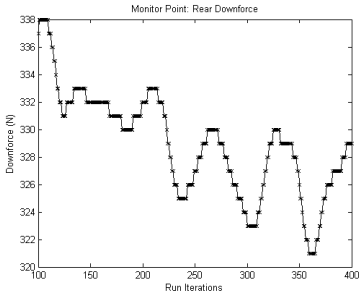
Monitor Point: Rear Downforce
Downforce (N)
Run Iterations

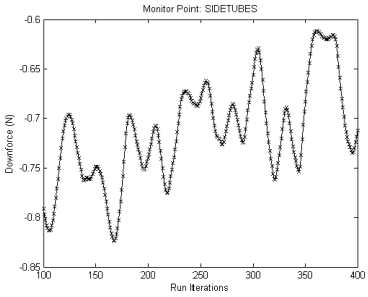
Monitor Point: SIDETUBES
Downforce (N)
Run Iterations

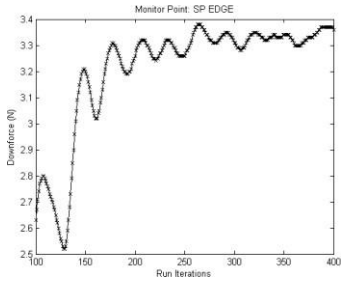
Monitor Point: SP EDGE
Downforce (N)
Run Iterations

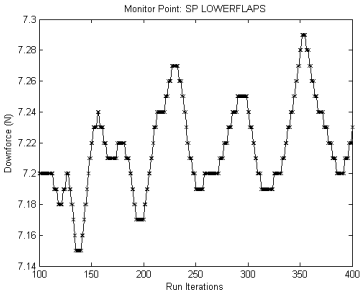
Monitor Point: SP LOWERFLAPS
Downforce (N)
Run Iterations

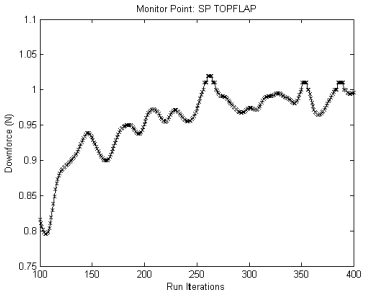
Monitor Point: SP TOPFLAP
Downforce (N)
Run Iterations

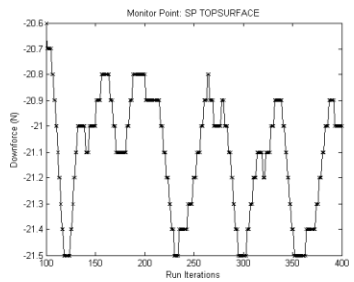
Monitor Point: SP TOPSURFACE
Downforce (N)
Run Iterations

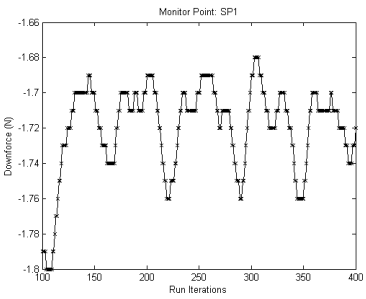
Monitor Point: SP1
Downforce (N)
Run Iterations

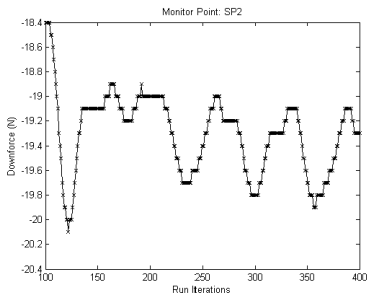
Monitor Point: SP2
Downforce (N)
Run Iterations

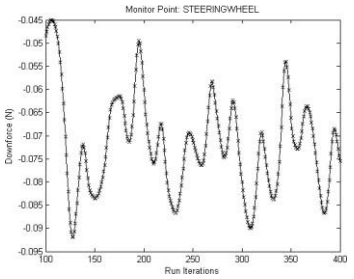
Monitor Point: STEERINGWHEEL
Downforce (N)
Run Iterations

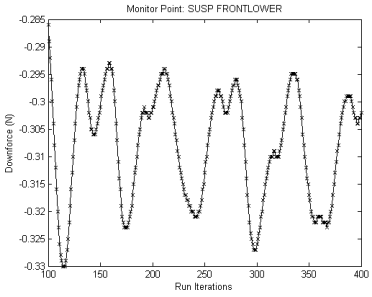
Monitor Point: SUSP FRONTLOWER
Downforce (N)
Run Iterations

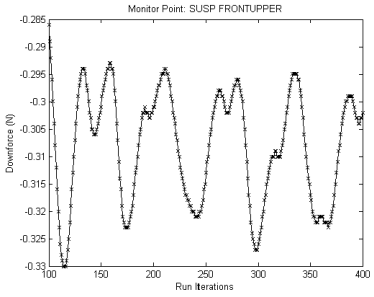
Monitor Point: SUSP FRONTUPPER
Downforce (N)
Run Iterations

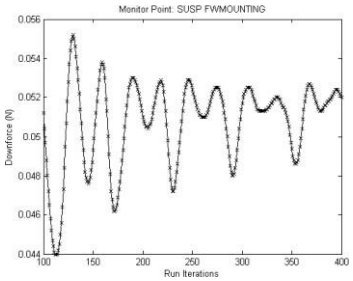
Monitor Point: SUSP FWMOUNTING
Downforce (N)
Run Iterations

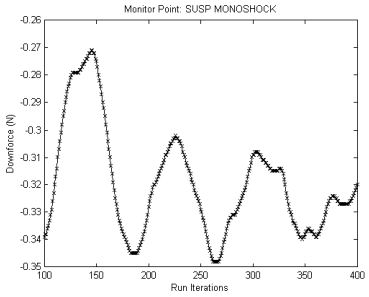
Monitor Point: SUSP MONOSHOCK
Downforce (N)
Run Iterations

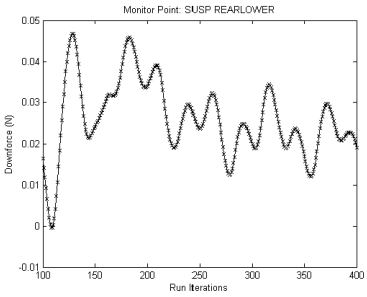
Monitor Point: SUSP REARLOWER
Downforce (N)
Run Iterations

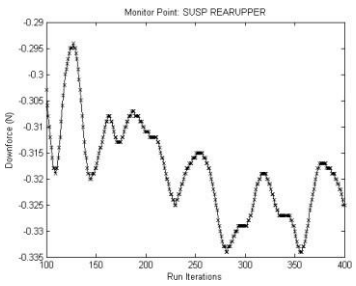
Monitor Point: SUSP REARUPPER
Downforce (N)
Run Iterations

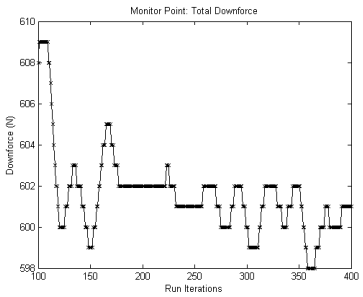
Monitor Point: Total Downforce
Downforce (N)
Run Iterations

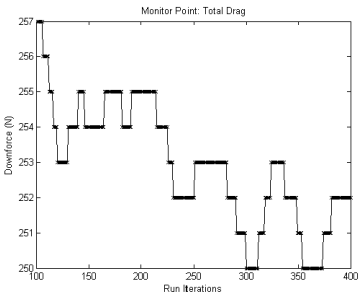
Monitor Point: Total Drag
Downforce (N)
Run Iterations

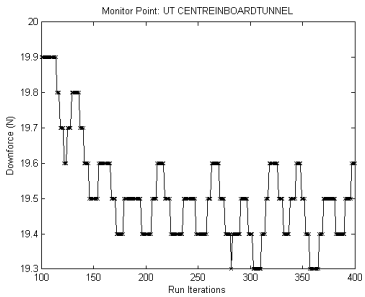
Monitor Point: UT CENTREINBOARDTUNNEL
Downforce (N)
Run Iterations

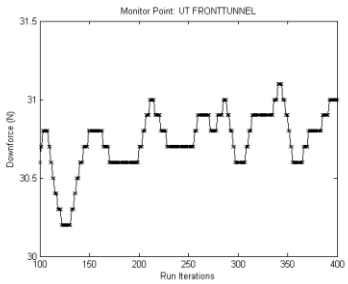
Monitor Point: UT FRONTTUNNEL
Downforce (N)
Run Iterations

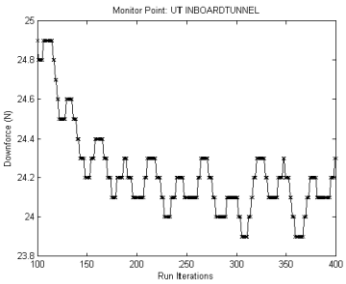
Monitor Point: UT INBOARDTUNNEL
Downforce (N)
Run Iterations

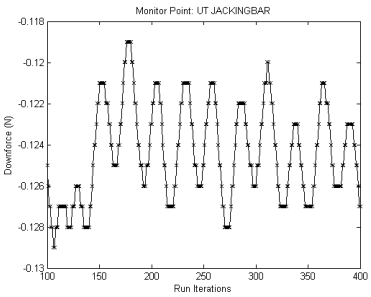
Monitor Point: UT JACKINGBAR
Downforce (N)
Run Iterations

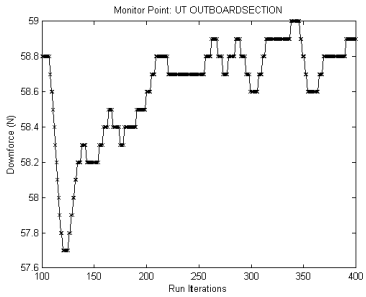
Monitor Point: UT OUTBOARDSECTION
Downforce (N)
Run Iterations

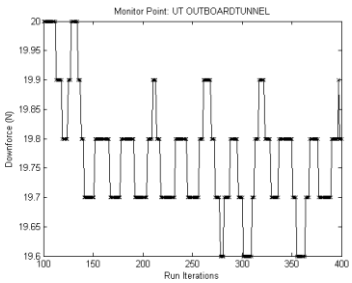
Monitor Point: UT OUTBOARDTUNNEL
Downforce (N)
Run Iterations

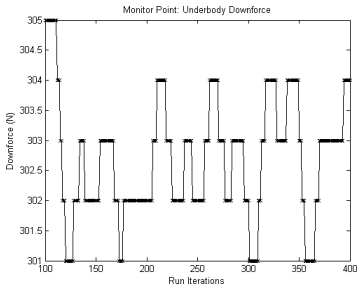
Monitor Point: Underbody Downforce
Downforce (N)
Run Iterations

11.3 New CFD Run Template

Upload to the Wiki once completed

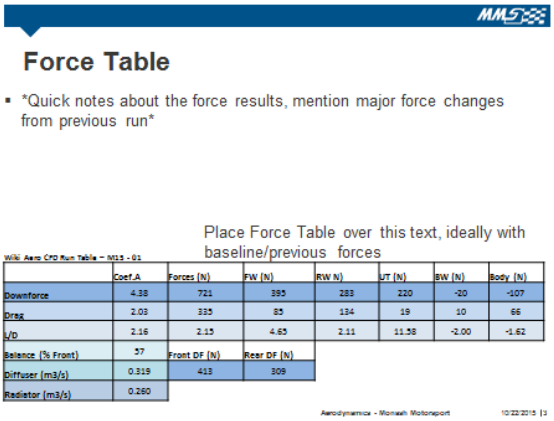

Wiki Aero CFD Run Table – M15 - 01

	Coef A	Forces (N)	FW (N)	RW N)	UT (N)	BW (N)	Body (N)
Downforce	4.38	721	395	283	220	-20	-107
Drag	2.03	335	85	134	19	10	66
L/D	2.16	2.15	4.65	2.11	11.58	-2.00	-1.62
Balance (% Front)	57	Front DF (N)	Rear DF (N)				
Diffuser (m3/s)	0.319	413	309				
Radiator (m3/s)	0.260						

Result Discussion *Duplicate*

- *Type as you discuss results*

- Place pictures/screenshots over this text

Recommendations for Next Run

- *Recommendations for next run, describe in as much detail as possible*

- Place diagrams/paint/quick CAD/sketches that describe the next change over this text

11.4 Size of Aerodynamics CFD Run Folder

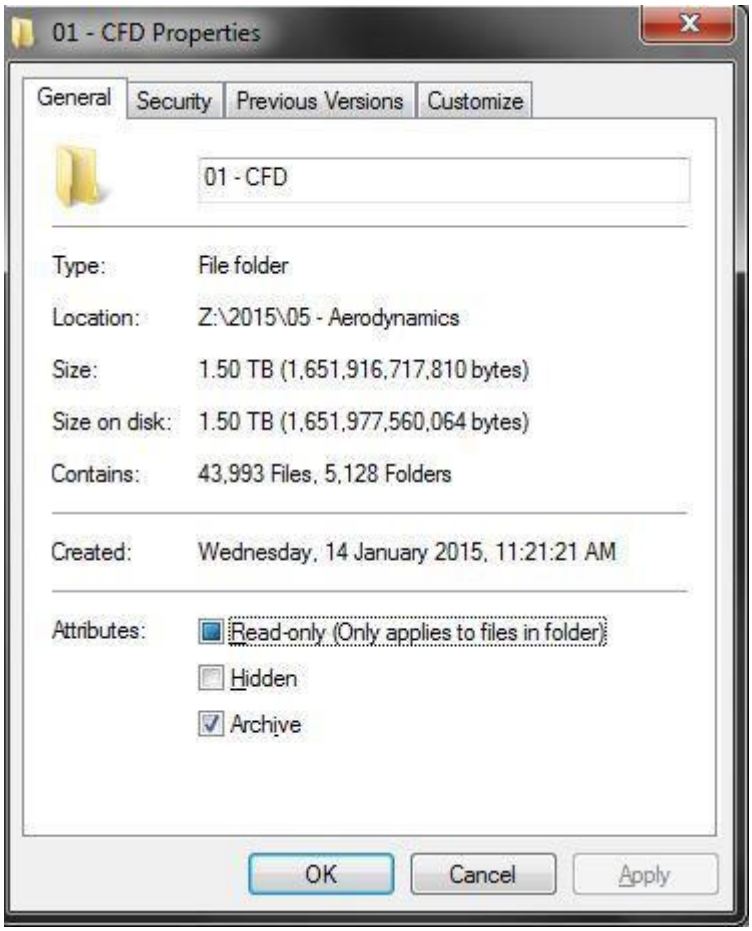

11.5 Ahmed Body

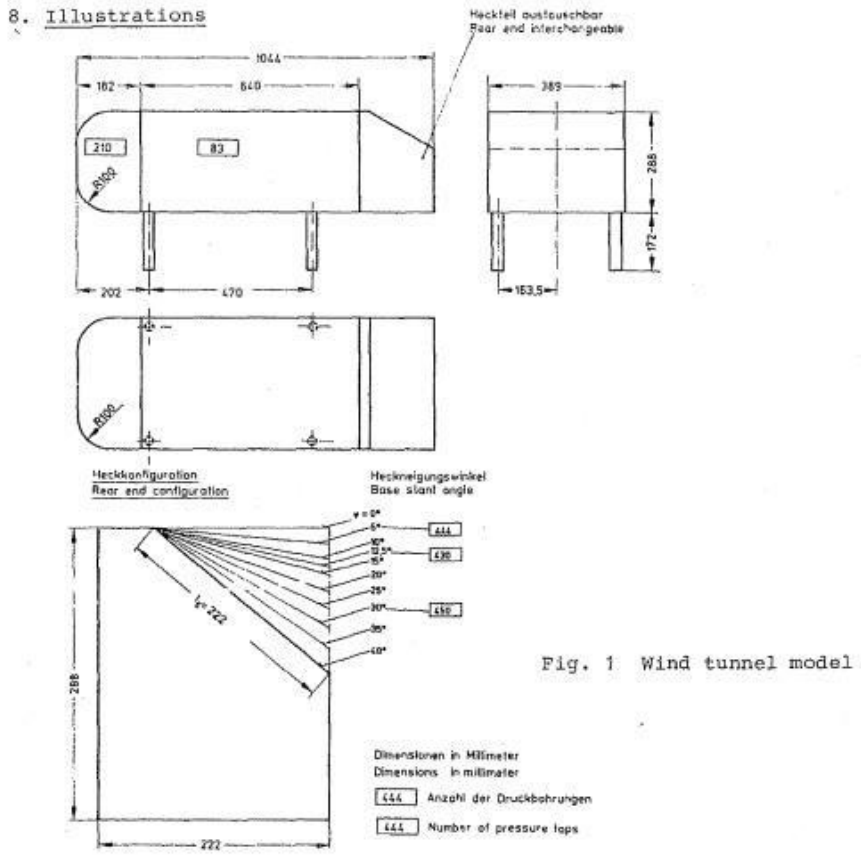

Fig. 1 Wind tunnel model

11.6 Domain Studies

Domain Studies											Momentum at Walls		
Area Change	Run No.	Change	Elements (million)	Solve Time (Hours)	Downforce (N)	Dragforce (N)	FW (N)	RW (N)	UT (N)	Body	X	Y	Z
Nearfield	02	Width, Slant	19.321	18.53	568	254	152	196	330	-100			
Nearfield	03	Width 1375mm	19.561	18.97	617	249	248	183	305	-108	0	148	-103
Nearfield	04	Width 1000mm	17.676	16.95	606	243	248	180	297	-106			
Nearfield	05	Width 1750mm	20.653	19.3	607	243	247	180	299	-106	0	132	-93
Nearfield	06	Height 2500mm	22.173	25.85	608	245	247	181	299	-106	0	132	-94
Nearfield	07	Height 1750mm	19.664	24.47	605	245	249	181	294	-105	0	133	-94
Nearfield	08	Height 1500mm	19.013	23.62	609	245	249	183	298	-107	0	136	-95
Nearfield	09	Height 2250mm	21.397		608	244	248	179	297	-104	0	130	-92
Nearfield	10	Width 2250mm	22.983		625	255	248	190	306	-109	0	149	-105
Wake	01	No Wake	17.753	15.37	613	248	249	184	302	-108	0	192	-111
Wake	02	Length 5000	19.903	18.42	622	251	248	185	306	-108			
Wake	03	Length 3000	18.26		610	245	249	182	299	-107	0	158	-99
Wake	04	Length 10000	21.824		609	246	249	182	297	-105	0	126	-92
Wake	05	Width 2000	19.175		609	244	247	181	300	-107	0	129	-92
Wake	06	Width 1000	20.946	17.76	622	257	245	191	306	-109	0	150	-105
Wake	07	Height 50mm	19.737		622	255	247	189	304	-108	0	146	-103
Wake	08	Height 1000	21.094		618	250	248	186	306	-110	0	150	-103
Wake	09	Matched To Wak	22.378		621	262	220	200	317	-106	0	159	-109
Farfield	01	Width Smaller	21.091		630	254	248	194	312	-112	0	209	-106
Farfield	02	Width Larger	21.218	21.283	620	255	243	190	306	-109	0	77	-107
Farfield	03	Length Shorter	21.119		618	255	244	188	305	-108	0	209	-133
Farfield	04												
Farfield	05	Height Lower	21.031	21.07	630	260	249	194	307	-110	0	149	-205
Farfield	06	Height Higher	21.176		615	248	248	183	304	-110	0	148	-51
Baseline	169	M15-169	22.36		614	250	245	184	302	-106			
Baseline	169	Re-run											
Domain Studies	169	Small No Wake	14.756	13.5	620	255	246	184	304	-104	0	113	-121
Domain Studies	169	Large	22.009	22.92	612	250	244	183	302	-106	0	98	-113
Domain Studies	177	Small No Wake	14.829		626	260	247	194	307	-110	0	51	-59
Domain Studies	177	Large	21.314	22.25	617	252	245	184	304	-105	0	36	-50
Domain Studies	169	Small No Wake											
Domain Studies	207	Small No Wake											
Domain Studies	207	Large											
Baseline	177	M15-177	22.38		620	261	220	199	316	-106			

11.7 Rotating Reference Frame Setup Spreadsheet

Rotating Reference Frame Calculations

INPUTS

Car Parameters (M15)		
Wheel Radius	228.6	mm
Wheel Width	240.5	mm
Front Track	1100.103	mm
Rear Track	1054	mm
Wheelbase	1550	mm
Cone Gap	50	mm

Auscomp Skidpad			
	2014	2013	
Time	4.8664	4.78	s
	0.2054907	0.209205	revs per s

Corner Radius			**Inverse Corner Radius**	
Aus SP Motec R	7.69E+03	mm	0.13	1/m
Aus SP Motec L	1.03E+04	mm	0.097	1/m
Aus Skidpad	7.63E+03	mm	0.000131	1/m
FSG Sweeper	1.67E+04	mm	0.06	1/m
FSG Cone Killer	2.00E+04	mm	0.05	1/m
FSG Slalom	1.25E+04	mm	0.08	1/m
FSG HW Hairpin	7.14E+03	mm	0.14	1/m
FSG Pendulum	3.33E+04	mm	0.03	1/m

Rotation Point 2015	FL	FR	RL	RR
Aus Skidpad	7795.25	8895.353	7970.467	9006.677
FSG Sweeper	17216.718	18316.82	17309.31	18359.32
FSG Cone Killer	20527	21627.1	20608.42	21659.58
FSG Slalom	15289	16389.1	15390.3	16439.29
FSG HW Hairpin	7172.7235	8272.827	7360.821	8394.122
FSG Pendulum	33333.539	34433.64	33392.58	34445.48

Steered Angle		
Aus Skidpad	25	degree
FSG Sweeper	14	degree
FSG Cone Killer	11	degree
FSG Slalom	9.1	degree
FSG HW Hairpin	15	degree
FSG Pendulum	9	degree

Corner Speed			**Lateral G's**	
Aus Skidpad	40	km/h	Aus Skidpad	1.4

FSG Track

Reference Map

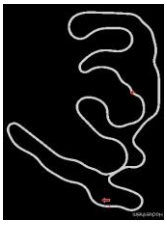

FSG Slalom

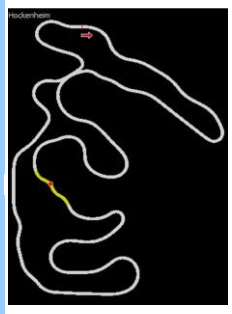

FSG Sweeper

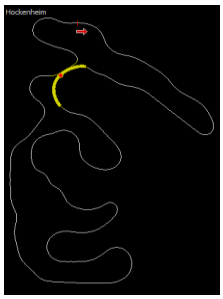

FSG Cone Killer Chicane

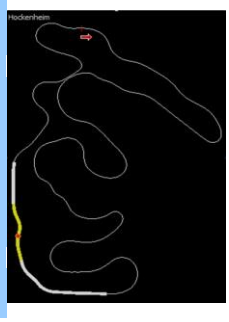

FSG Pendulum

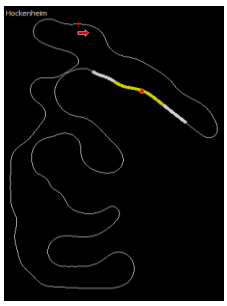

11.8 Wind Tunnel Testing Report

Date: 6 - 9 th October
Test Vehicle: M15
People in charge:
Team Members Present:
Location: Monash Full-Scale Wind Tunnel
Test plan by: Ryan

Motivation for Testing:

The 2015 rules reduced the span of the rear wing and hence limits the performance of the rear wing. Using CFD to design endplates showed that with considerable difference in pressure contours there was not a noticeable change in force numbers. This, in conjunction with most of the time spent determining rear wing position/flap angles/slot gaps and unsprung mounted endplates, resulted in not

many CFD simulations on the endplates.

Given this result, wind tunnel testing has shown in the past to show good results in rear wing performance indicators. Therefore the main focus of the tunnel testing will to be improve the performance of M15 through endplate design and rear wing positioning.

M14 with profiled endplates. Showed big gains at 20 deg (which it doesn't see), still might be worth looking at.

To determine the performance of the aero package, the test will use the kistlers (force sensors from the tunnel) to determine forces and flow vis/wool tuffs/smoke to visualise flow structures. Pressure tapping is planned to be ready before the tunnel in both mainplanes of front and rear wings.

Ryan is planning to use data for FYP to improve CFD model, so determining pressures and flow structures in the tunnel will be beneficial.

Design data is useful for both design event and future years. Therefore pressure mapping the wake, reverse/spin cases and

Enter testing idea screenshot here:

Safety:

All team members wishing to take part in the test or to enter the tunnel will be required to attend a safety induction in the tunnel before testing commences. Members who do not receive this induction must remain in the control room.

Inducted members will be required to sign a hard copy of the safety induction sheet to be left for the wind tunnel manager at the end of the testing session.

This will be strictly enforced - no one will be allowed to enter the testing section unless they have done the induction and signed the form.

Last year there was an incident concerning the groundplane not being properly secured. Sandbags are available to weigh the groundplane down but more importance will be put on securing with fasteners before tunnel testing.

Each new design change or setup change must be checked off by two people - one of which is supervisor and the other the person in charge of the testing.

All members must be responsible for cleaning up regularly throughout the entire testing session.

Members who are tired (sleep deprived) will go home or have a nap as this is where incidents can occur.

Safety procedures will be attached at the bottom of this page and a printed copy in a clear folder will be present at testing.

Test metrics:

Testing will be successful if improvements in the 2015 aero package are made and all data is recorded on the wiki and reviewed.

If no gains are found in this process, all data must be recorded and reviewed for a semi-successful testing.

Using Cam Warne's testing metric system, performance of the team will also be recorded. See Testing Metrics.

Preparation will be a massive performance indicator for the team, as in the past being under prepared for the wind tunnel has severely affected time spent in the tunnel and the number of tests completed. Having the car fitted with groundplane in position on a mock turning table before the testing begins is the best preparation.

Test Layout:

The car will be mounted to the new wind tunnel rig, which uses the Suzuki kistlers which are smaller track width and wheelbase then previous years.

Therefore a new ground plane will be made to fit the rig. The variable height struts need modifications in order to fit the span of the rear wing and this will be completed before testing.

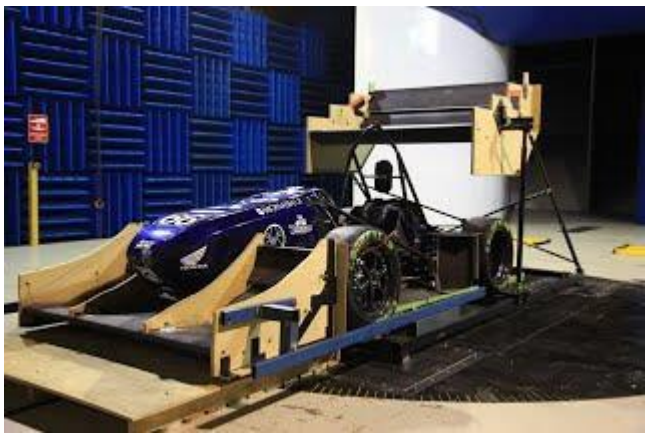

Specific points will be marked out for photos of changes.

The same will be done for points to take of smoke vis and flow vis.

Baseline:

Start of each day a baseline run (including one without the car if any modifications have been made to groundplane/rig) must be done.

Do a yaw sweep to 12 degrees in increments of 3 (3 - 6 - 9 - 12).

Monitor conditions - such as temperature - that could effect baseline other than modifications to the car or test rig

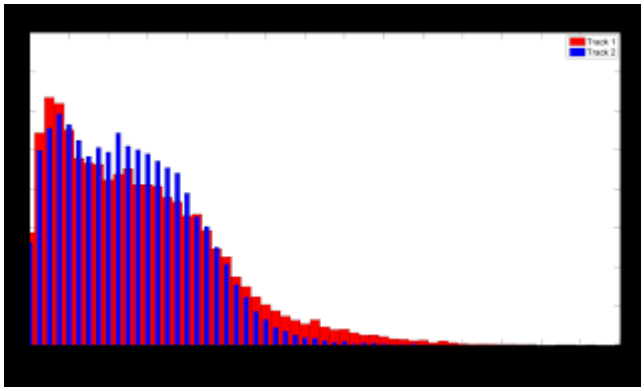

What we will need:

M15

- Wiring secured with cable ties/tape
- Engine bay cleaned
- All tyres cleaned of rocks/dirt
- Bolt check completed
- Flow tripper for tyres

Rig

- Wing struts
- Groundplane
- Endplate attachment struts

Flow Vis Pack

- Vicome
- Kerosene
- Baby Powder
- Portable spray gun
- Tarp
- Mop
- Cleaning cloths
- Wool tuffs

Tools

- Racetape
- Cable ties
- Plywood
- Screws
- Drill
- Jigsaw
- Sanding paper
- Files
- Broom
- Vacuum (provided by Wind Tunnel)

Misc

- Testing Plan
- Risk Assessment forms
- Radios
- Eating schedule (Ryan to organise food and attach spreadsheet at bottom)
- Camera
- GoPro

Test Schedule:

Session Number - Test Number - Title

ie For rig baseline, session number 01, test 04, yawed at 15 degrees = 01-04-Rig Baseline Yaw15

Session Number	Title	Description	Yaw Sweep
01	Rig Baseline	Rig Baseline	Y
02	M15 Baseline	M15 Baseline	Y
03	Reynolds Sweep	See if Reynolds number affects flow structures/force	N
04	Rear Wing Position	See best x location for wing	N
05	Rear Wing AoA	Best RW AoA	N
06	Rear Wing Endplate Design	Change sections of endplate to see improvements for M15 EP	Y 0-5
07	Further Rear Wing Design Improvements	Any other ideas related to improving RW performance	N
08	Driver Height Sweep	Bartlett - Ryan - Roseann	N
09	CFD ideas	Any designs that showed difference in performance during design period	Y
10	Pressure Tap Wings	Put on car and get results	N
11	Smoke and Flow Vis	Include Rad and Inter in this to see what flow structures get there	Y
12	Steered Wheels	Also get smoke for this	Y
13	Design Data	Reverse/Spin/Cross wind modes, see if we can get rear wake pressure mapping	Y

11.9 Wind Tunnel Schematic